The ternary phase diagram Sb-Sn-Ti

Patric Berger, Clemens Schmetterer, Herta Effenberger, Hans Flandorfer

PII: S0925-8388(21)01681-9

DOI: https://doi.org/10.1016/j.jallcom.2021.160272

Reference: JALCOM160272

To appear in: *Journal of Alloys and Compounds*

Received date: 23 February 2021
Revised date: 20 April 2021
Accepted date: 29 April 2021

Please cite this article as: Patric Berger, Clemens Schmetterer, Herta Effenberger and Hans Flandorfer, The ternary phase diagram Sb-Sn-Ti, *Journal of Alloys and Compounds,* (2021) doi:https://doi.org/10.1016/j.jallcom.2021.160272

The ternary phase diagram Sb-Sn-Ti

Patric Berger[1)], Clemens Schmetterer[2)], Herta Effenberger[3)] and Hans Flandorfer[1)]*

1) University of Vienna, Faculty of Chemistry, Institute of Inorganic Chemistry – functional Materials, Althanstraße 14, 1090 Vienna, Austria
2) University of Vienna, Faculty of Chemistry, Institute of Physical Chemistry, Waehringerstraße 42, 1090 Vienna, Austria
3) University of Vienna, Faculty of Geosciences, Geography and Astronomy, Institute of Mineralogy and Crystallography, Althanstraße 14, 1090 Vienna, Austria

*- corresponding author: hans.flandorfer@univie.ac.at

Abstract:

The ternary intermetallic compound SbSnTi is known for a reversible uptake of Li at low potentials versus pure Li and is therefore a candidate as anode material for use in Li-ion batteries (LiBs). Up to now, no phase diagram data for the ternary Sb-Sn-Ti system have been reported in literature, which is, however, crucial for the understanding of the lithiation process. In this work isothermal sections of this system at 600 °C, 800 °C and 1000 °C were acquired for the first time. They are based on powder X-ray diffraction (PXRD) and scanning electron microscopy (SEM/EDX) investigations of alloy samples. During our investigations two new ternary phases, $Sb_xSn_{19-x}Ti_{15}$ and $(Sb_xSn_{1-x})_{3-y}Ti_{5+y}$, were recognized from PXRD patterns; the crystal structures were subsequently determined by single-crystal X-ray diffraction. $Sb_xSn_{19-x}Ti_{15}$ crystallizes with the cubic space group *Pm*-3 (No. 200), the lattice parameter is a = 8.8502 Å. $(Sb_xSn_{1-x})_{3-y}Ti_{5+y}$ shows tetragonal symmetry with the lattice parameters a = 10.553 Å and c = 5.3982 Å and the space group *I*4/*mcm* (No. 140). A further ternary compound, Sb_4SnTi_5, could be identified; its incommensurable crystal structure could not yet be fully described.

Keywords

intermetallics, phase diagrams, X-ray diffraction, crystal structure

1. Introduction

Ternary alloys of the composition SbSnTi [1] have been found to be prone for reversible electrochemical lithiation [2-9]. According to the study of Sougrati and co-workers [2], electrochemical lithiation of SbSnTi leads to a conversion reaction forming Li-Sb and Li-Sn alloys during the first discharge process in which pure Ti is precipitated simultaneously. Thereby, Li_3Sb and Li_7Sn_2 represent the respective highest lithiated phases [2]. Both, Sb [10] and Sn [11], are active towards lithiation, whereas Ti is inactive and serves as buffer of mechanical stress during the lithiation process. Furthermore, the lithiation mechanism on cycling of SbSnTi anodes[1] was studied by Marino et al. [3] performing in-situ XRD, ^{121}Sb, ^{119}Sn Mössbauer spectroscopy and ^{7}Li NMR measurements. While the lithiation of SbSnTi during the first discharge process reported by Sougrati et al. [2] was largely confirmed, the reaction scheme during the charge process (delithiation) differs. Thereby, Sougrati and co-workers [2] expected the formation of Sb-Ti, Sn-Ti and also ternary Sb-Sn-Ti alloys. On the contrary, Marino et al. [3] reported about the formation of SbSnTi in addition to small amounts of Li_3Sb at the end of the first charge process. However, all such investigations suffer from the absence of phase diagram information on the respective higher order alloy systems. To understand, control and predict reaction pathways in such systems, the knowledge on phase equilibria, thermal behavior, crystal structures and thermodynamic properties is necessary:

- phase equilibria allow the deduction and interpretation of the stepwise lithiation processes in terms of phases that can be formed.
- crystal structures, densities and molar volumes of phases allow the estimation of the lithiation mechanisms, diffusion pathways and volume changes upon (de)lithiation.
- thermodynamic properties are directly linked to the open circuit voltages and thermal behavior.

In this article we present the results of the investigation of the ternary Sb-Sn-Ti system obtained by the application of PXRD and SEM/EDX. Three isothermal sections at 600 °C, 800 °C and 1000 °C were derived from the collected data. Additionally, the two new ternary phases $Sb_xSn_{19-x}Ti_{15}$ and $(Sb_xSn_{1-x})_{3-y}Ti_{5+y}$ were characterized by single-crystal X-ray diffraction. A further ternary phase, Sb_4SnTi_5, was isolated and a basic crystallographic description is given.

[1] it represents the cathode on lithiation against Li-metal

However, it shows incommensurability and a proper single crystal, which allows a full description of the modulation, was not yet found.

2. Literature review

2.1. Sb-Sn

Phase diagram information of this system has been taken from Schmetterer et al. [12, 13], who reviewed and assessed literature data in detail [12] and established a new phase diagram version based on the own experiments and the conclusions from the literature study [13]. According to this phase diagram, the compounds SbSn and Sb_3Sn_4 show a certain homogeneity range, whereby the one of SbSn shows a maximal extension of around 15 at.% at 326 °C and Sb_3Sn_4 a maximal extension of 2.5 at.%. The maximum solubility for Sn in (Sb) was estimated to be around 13 at.% at 425 °C, while the one for Sb in solid (Sn) is around 10 at.% at 244 °C. The three peritectic reactions L + (Sb) → SbSn at 425 °C, L + SbSn → Sb_3Sn_4 at 326 °C and L + Sb_3Sn_4 → (Sn) at 244 °C are based on DTA measurements.

These authors clarified a number of uncertainties and inconsistencies which appeared in literature; only a brief summary of their findings can be given here – for details please see [12] and [13].

- The proposed incommensurate crystal structure and the large homogeneity range of SbSn [14] was confirmed; however, the existence of a high and a low temperature modifications of this phase as reported by Hansen and Anderko [15] could not be verified.
- The occurrence of an invariant reaction at 326 °C was confirmed; it is the peritectic formation of the new compound Sb_3Sn_4 (L + SbSn → Sb_3Sn_4). The existence of this compound was first proposed by Stegherr [16], but not elaborated in detail; his phase diagram suggestion also reports a small miscibility in SbSn.
- Schmetterer et al. [13] showed that Sb_3Sn_4 is a commensurate superstructure of the basic SbSn structure. SbSn and Sb_3Sn_4 were interpreted as two independent phases (separated by a tentatively developed small two-phase field). The immiscibility in SbSn was not confirmed in their work [13].
- The existence of a further compound Sb_2Sn_3 was ruled out by Schmetterer et al. [13]; this compound had been reported in numerous studies (e.g. [17-19]) and should crystallize in a NaCl structure. These reports had been spawned by early microstructural investigations using light microscopical studies, where a variable morphology of crystals with the

average composition "SbSn" depending on the relative Sb:Sn ratio had been reported (cubic on the Sn-rich side, minor rhombohedral distortion on the Sb-rich side).

Later, Sb_2Sn_3 got introduced into the system to explain the invariant reaction at 326 °C and was assigned the NaCl-structure; various different phase diagram versions comprising both compounds were published: e.g. according to Okamoto [19] and Chen et al. [18], Sb_2Sn_3 is stable down to room temperature. Based on earlier works by Predel and Schwermann [20] as well as Massalski [17], the stability ranges between 250-324 °C. However, such a compound was never isolated or structurally characterized. Schmetterer et al. [13] reported that the rhombohedral angles of the trigonal unit cell for the "SbSn" structure-type vary and get close to 90° on the Sn-rich side of the solid solution, but the unit cell never becomes cubic.

The most recent experimental investigation in terms of thermal analysis, metallography and XRD was published by Borzone et al. [21]. Their results confirm the one of Schmetterer et al. [13] in a wide extent. Two very recent thermodynamic assessments were published by V.A. Lysenko [22] and W. Gierlotka [23]. The latter one includes also ab-initio calculations of the enthalpy of formation of Sb_3Sn_4.

2.2. Sb-Ti

Investigations of the binary Sb-Ti system started in the middle of the last century, when Nowotny and co-workers [24-26] studied this system by means of PXRD and light optical microscopy. They claimed the existence of four intermetallic compounds (Ti_4Sb, $Ti_{2.5}Sb$, TiSb and $TiSb_2$). Shortly afterwards, Kjekshus et al. [27] characterized further four Sb-Ti alloys with individual structure types prepared by various melting technics (cubic and tetragonal Ti_3Sb and the two orthorhombic phases $Ti_{1.7}Sb$ and $Ti_{1.2}Sb$). (The tetragonal Ti_3Sb structure might be stabilized by impurities [28], caused by syntheses in alumina crucibles). However, these latter authors could not confirm the existence of the phases Ti_4Sb and $Ti_{2.5}Sb$ reported earlier [25, 26]. The orthorhombic phase $Ti_{1.7}Sb$ [27] was later identified as Ti_5Sb_3 [29], it is isotypic to β-Yb_5Sb_3.

One of the first critical assessments of the binary Sb-Ti system was done by Murray [30] in 1987; it is depicted in [17], which includes seven intermetallic phases: Ti_4Sb, Ti_3Sb (cubic and tetragonal), $Ti_{2.5}Sb$, Ti_5Sb_3, Ti_6Sb_5, TiSb and $TiSb_2$. Besides the melting temperatures of the pure elements, only that of $TiSb_2$ was considered based on investigations by Dudkin and Vaidanich [31] in 1960 and the peritectic reaction L + TiSb → $TiSb_2$ at 1010 °C. Thereafter, some

additional intermetallic phases in the binary Sb-Ti system were described: the new binary antimonide $Ti_{11-x}Sb_{8-y}$ was characterized by Bobev and Kleinke [32], Ti_5Sb_8 was found by Zhu and Kleinke [33, 34], whereas Ti_2Sb was established by Derakhshan et al. [35].

We refer to the most recently reported phase diagram version of the Sb-Ti system by Tavassoli et al. [36]. In their extensive experimental study, they investigated this challenging system (due to large differences in various physical properties of Ti and Sb such as melting point and vapour pressure, etc.) by means of DTA, PXRD, single-crystal-XRD and SEM/EDX measurements of many arc-melted samples. Finally, their Sb-Ti phase diagram includes seven intermetallic phases. Six of them (Ti_3Sb, Ti_2Sb, $Ti_{11-x}Sb_{8-y}$, TiSb Ti_5Sb_8 and $TiSb_2$) arise from peritectic reactions, while Ti_5Sb_3 crystallizes congruently from the liquid phase. Only three Sb-Ti alloys show a distinct homogeneity range: Ti_3Sb (21.9-24.4 at.% Sb), $Ti_{11-x}Sb_{8-y}$ (41,9-43 at.% Sb) and TiSb (49.5-50 at.% Sb), while the homogeneity range of all other phases was reported to be less than 0.3 at.%. The solid solubility of Ti in (Sb) was determined to be neclectable, while this of Sb in (Ti) increases from 7 at.% Sb at 600 °C up to 11 at.% Sb at 1306 °C.

2.3. Sn-Ti

The first critical assessment of the binary system Sn-Ti was done by Murray [37] and is depicted in [17]. This phase diagram version comprises four intermetallic compounds Sn_5Ti_6, Sn_3Ti_5, $SnTi_2$ and $SnTi_3$. $SnTi_2$ and $SnTi_3$ show a significant homogeneity range, which rises with increasing temperature for $SnTi_2$ (up to 32.7-39.9 at.% Sn) and for $SnTi_3$ (up to 23-25 at.% Sn); Sn_5Ti_6 is polymorphic and shows a phase transformation from α-Sn_5Ti_6 (space group: *Immm*) to β-Sn_5Ti_6 (space group: $P6_3/mmc$) at 790 °C. Both titanium modifications, α-Ti and β-Ti, exhibit a significant solid solubility of Sn; it is larger for β-Ti (~17 at.% Sn) than for α-Ti (~13 at.% Sn). β-Sn_5Ti_6 and $SnTi_3$ both crystallize congruently from the liquid phase, whereas Sn_3Ti_5 and $SnTi_2$ are formed by peritectic reactions at ~1510 °C and 1550 °C, respectively.

In 1998, Kuper and co-workers [38] restudied the binary Sn-Ti system in the composition range of 29-88 at.% Sn based on XRD, SEM and EDX methods. During their work they observed a new intermetallic compound, with a composition of approx. 60 at.% Sn (later confirmed by O´Brien [39]), which is stable up to at least 700 °C, but presumably not higher than 770 °C. The authors associated the formation of this compound with a peritectic reaction of L + Sn_5Ti_6 → Ti_2Sn_3. An uncertainty with respect to the phase transformation of α/β-Sn_5Ti_6 remained; Kuper et al. [38] reported two tentative possibilities: (i) down to room temperature β-Sn_5Ti_6 is stable and

α-Sn_5Ti_6 is metastable, or (ii) a phase transformation occurs at temperatures lower than 670 °C. Nevertheless, their published phase diagram contains both α- and β-Sn_5Ti_6, but the phase transition is indicated by a dashed line.

Recently, Bondar et al. [40] studied an alloy $Sn_{18.5}Ti_{81.5}$ by DTA and reported a temperature of 1575 °C for the eutectic reaction L → (βTi) + $SnTi_3$, which is much lower than previous literature data, e.g. Murray [37] published 1605 °C in his phase diagram version.

An early thermodynamic assessment of the Sn-Ti system based on the CALPHAD method was done by F. Hayes in 1992 and published in [41]. Newer assessments including also the most tin-rich phase Sn_3Ti_2 were provided by Liu et al. [42], Yin et al. [43] and Wang et al. [44] with the aim of extrapolations into higher-order systems. All three versions exhibit similarities in their general outline (e.g. number of intermetallic compounds), but they differ significantly in the shape of the liquidus, the homogeneity ranges of some phases and the α/β-Sn_5Ti_6 phase transformation.

Especially, at the Sn-rich side, the slope of the liquidus differs in the published Sn-Ti phase diagram versions [37, 42-45]. DTA studies in the Sn-rich corner were carried out by Eremenko and Velikanova [46] to determine the liquidus in this part of the Sn-Ti system. Later on, Yin et al. [43] complemented these DTA measurements. Plevachuk et al. [47] performed electrical conductivity and viscosity measurements of the liquid phase in a concentration range of 50-100 at.% Sn. All these results are considered and combined in the calculated Sn-Ti system phase diagram of Wang et al. [44], which is taken as a basis for the present studies.

2.4. Sb-Sn-Ti

To the best knowledge of the authors, up to now no information on the phase equilibria in the ternary system Sb-Sn-Ti is available in literature. Only the existence and crystal structure of a pseudo-binary and a ternary compound have been reported by [1, 48, 49].

3. Experimental

3.1. Sample preparation

Most samples were prepared by conventional arc-melting of stoichiometric amounts of Sb-Sn master alloys with pure titanium on a water cooled Cu mount under zirconium gettered

argon atmosphere. Pure titanium rods (Alfa Aesar, 99,99%), tin rods (Alfa Aesar, 99,9985%) and Sb ingots (Alfa Aesar, 99,999%) were used as starting materials. Before use, Sb was purified by filtration of the liquid metal through quartz glass wool under vacuum. Titanium and tin were used as purchased.

To compensate the mass loss of antimony during the arc-melting procedure, an excess of around 1.5 wt.% Sb was added to all samples containing more than 40 at.% Sb. The actual composition of each sample was determined by SEM-EDX area scans, listed in Tables 2s-4s in the supplementary material. Particularly Sb-rich alloys were prepared from arc-melted Sb-Ti and Sb-Sn master alloys, which were crushed into fine powders, mixed, cold pressed into pills and finally, arc-melted.

In a final step the samples were placed in alumina crucibles, sealed in quartz glass tubes under vacuum and annealed in a muffle furnace at 600 °C, 800 °C and 1000 °C, respectively. In order to freeze the high temperature equilibrium, samples were quenched in cold water. Characterization of each sample was primarily done by powder X-ray diffraction (PXRD) and scanning electron microscopy (SEM/EDX). In addition, selected samples were further investigated by light optical microscopy (LOM).

3.2. Powder X-ray diffraction (PXRD)

Powder diffractograms were recorded on a Bruker-D8 diffractometer with Bragg-Brentano pseudo-focusing geometry (θ/2θ geometry) with $Cu_{K\alpha}$ X-radiation (40kV/40 mA) and a Ni filter. Detection of the scattered intensities was carried out using a one-dimensional Si-strip detector (LynxEye detector, Bruker, Germany). Therefore, small amounts of alloys were powdered using either a Durit®mortar or, in case of ductile Sn-rich alloys, a diamond file. Powders of alloy samples, simultaneously poor in Sb and rich in Ti, were further stress annealed at the corresponding annealing temperature for around 20 minutes. For the measurement, the powders were attached with petroleum jelly on a silicon single-crystal sample holder. For phase identification full profile Rietveld-refinement was generally applied using Topas4®software.

3.3. Single crystal X-ray diffraction (SCXRD)

During the investigations by PXRD and SEM, two new ternary phases, $Sb_xSn_{19-x}Ti_{15}$ and $(Sb_xSn_{1-x})_{3-y}Ti_{5+y}$, were recognized. They were subsequently characterized by single-crystal structure determinations. In both cases multiple trials were necessary to find a single crystal of

sufficient quality for X-ray data collection. Small but irregular crystal chips of the title compounds were mounted on thin glass capillaries. Reflection intensities were collected with a four-circle Nonius Kappa diffractometer (CCD detector, 300 µm capillary optics collimator, conventional X-ray tube, monochromated MoKα radiation). The unit-cell parameters were determined by least-squares refinements from the 2θ values of the positions of the measured Bragg reflections. Corrections for Lorentz, polarization and absorption effects (multi-scan method) were applied; complex scattering functions [50] were used. For data collection, structure solution and refinements served the programs "Collect" [51, 52], "SHELXS-97" and "SHELXL-97" [53-56]. Details about crystal data, single crystal X-ray data collection and refinements of the crystal structures are given in Table 1. Table 2 summarizes the atomic coordinates and displacement parameters, Tables 3 and 4 selected interatomic bond distances. The display of the crystal structures is based on the software ATOMS [57].

Results from structure refinement are limited to a refinement of Ti and *M* = (Sn,Sb) atoms as tin and antimony are neighbored in the periodic table and their similar scattering power prevents a clear distinction based on conventional X-ray sources. Only in a few cases some improvement of the structure refinement was obtained for distinct occupations by Sb and Sn atoms, respectively [48, 58]. Furthermore, the formation of vacancies and substitutions of M by Ti atoms at the same site are experimentally not distinguishable. Therefore, the stoichiometry of the new crystal structures was established in combination with EDX analyses.

3.4. Scanning electron microscope (SEM)

Studies of the microstructure of the alloys were performed by scanning electron microscopy (Zeiss Supra 55 VP ESEM, acceleration voltage 20 kV, beam current 10 nA), in addition to light optical microscopy. The respective phases were chemically analyzed by energy dispersive X-ray spectroscopy (EDX). The quantification of element concentrations is based on previous standard measurements and energy calibration of the EDX signal using a cobalt-standard.

For SEM/EDX investigations, pieces of samples were embedded in carbonized phenolic hot mounting resin and further grained using SiC papers from 240 to 2000 mesh. The samples surfaces were further polished with an Al_2O_3 slurry of 1 µm and inspected with a light optical

microscope in order to identify remaining scratches. After the polishing process, molds were finally cleaned in an ultrasonic bath of distilled water and then ethanol.

4. Results and Discussion

4.1. The binary system Sn-Ti

The results of our investigations in the ternary Sb-Sn-Ti system were largely consistent with the binary systems Sb-Sn and Sb-Ti published earlier [13, 36] . However, inconsistencies concerning the homogeneity ranges of corresponding binary Sn-Ti phases were noticed in some cases, where in particular the ternary solid solutions of $SnTi_3$ and Sn_5Ti_6 showed much higher solid solubilities towards the Ti-rich side than reported for the corresponding binaries in the literature. Therefore, selected samples in the binary Sn-Ti system were prepared by conventional arc melting of the pure elements, annealed at different temperatures and quenched. Phase analyses of the binary Sn-Ti alloys are listed in Table 1s in the supplementary material, including heat treatment conditions, lattice parameters obtained for the distinct phases by Rietveld-refinements and chemical compositions from EDX. Based on our results of the binary Sn-Ti alloys, the phase diagram of Wang et al. [44] was adapted (see Fig. 1). In particular, the homogeneity ranges for Sn_5Ti_6 and Sn_3Ti_5, both hitherto described as line compounds, were extended by around 2 at.% towards the Ti-rich side for Sn_5Ti_6 and more than 1 at.% towards the Sn-rich side for Sn_3Ti_5. The greatest difference to Wang et al. [44] concerning the homogeneity range, however, was observed for $SnTi_3$, which shows a maximum solubility of more than 5 at.% towards the Ti-rich side. On the other hand, the maximum solid solubility of Sn in (Ti) is according to our experiments slightly lower as given by Wang et al. [44].

Additionally, it was our goal to determine the slope of the liquidus on the Sn-rich side based on two independent methods. On the one hand, DTA measurements of arc-melted samples with compositions between 60 and 95 at.% Sn were performed (heating rate 5 K/min). Thereby, the evaluation of a distinct liquidus temperature was not possible since the heat exchange extends over a very wide temperature range resulting in extremely broad peaks which merge with the baseline. This observation is not uncommon in case of very steep liquidus lines and slow inter-diffusion. On the other hand, drop calorimetry measurements by dropping Ti pieces (20-45 mg) in liquid Sn were carried out at distinct temperatures. Typically, the crossing of the liquidus can

be seen from a kink in the course of the heat effects with concentration, where the first solid phase forms (see our previous works e.g., on the Li-Sb-Sn system [59]). Unfortunately, this method has proven to be unsuitable for the Sn-Ti system since the Ti pieces have not dissolved completely. These observations, together with our difficulties to establish full equilibrium in binary and ternary samples on annealing, described below, indicate a quite slow inter-diffusion in such alloys, even so in the semi-liquid state.

4.2. The ternary system Sb-Sn-Ti

All results of PXRD and SEM/EDX were combined to establish the isothermal sections at 600 °C , 800 °C and 1000 °C, (see Figs. 2-4). The results of phase analyses for all samples annealed at various temperatures are compiled in Tables 2s-4s in the supplementary material; all detected phases, their lattice parameters obtained from full-profile Rietveld-refinements, their compositions as derived from EDX measurements, nominal compositions, and heat treatment conditions are included. The four ternary compounds SbSnTi, $(Sb_xSn_{1-x})_{3-y}Ti_{5+y}$, Sb_4SnTi_5 and $Sb_xSn_{19-x}Ti_{15}$ are indicated for short by T1, T2, T3 and T4, respectively, throughout this work.

For the details of the crystal structure of the compound T1 we refer to [1, 48]; T2 was predicted based on ab-initio calculations [60] and its existence could be confirmed by our experimental single-crystal investigations.

The compounds T3 and T4 have not been mentioned in literature up to now. We solved the crystal structure of T4 based on SCXRD while only a preliminary and average description of the incommensurate crystal structure of T3 can be given yet. In the second part of this work the crystal structures of these four ternary compounds are presented and discussed.

Several assumptions were made before starting with the construction of the isothermal sections. First, all binary phases, their binary solubilities as well as the shape of the liquidus were adopted from the three binary systems Sb-Sn [13], Sb-Ti [36] and Sn-Ti [44] as discussed above. The latter one has been slightly revised according to our investigation of binary samples, see Table 1s in supplementary material and Fig 1.

Although several attempts were made to determine the composition of the solidified liquid by SEM/EDX area scans on samples quenched from the partially liquid state at their annealing temperature, no significant result was achieved in most cases. Distinct areas of the

same samples show different compositions; this could be caused by coarse grain formations and segregations in crystallization of the liquid during the quenching process. Consequently, the results were not representative for the liquid composition.

However, due to an assessment of all partially liquid samples at the respective annealing temperatures, the most likely connection points of the corresponding phase fields with the liquidus were estimated and therefore depicted by dashed lines. As examples, in Fig. 5, the SEM-micrographs of three such pairs of two- and three-phase samples are shown. The two samples $Sb_{34.9}Sn_{38.3}Ti_{26.8}$ and $Sb_{33.8}Sn_{45.1}Ti_{21.1}$ were annealed at 800 °C. The first one in Fig. 5a consists of SbTi, T1 and solidified liquid and the second one in Fig. 5b indicates a two-phase equilibrium of T1 and solidified liquid only. From this information it was possible to localize the tie-line which separates the three-phase field [SbTi + T1 + L] from the two-phase field [T1 + L]; see Fig. 3. Similar examples are shown in Figs. 5c, d and Figs. 5e, f respectively, for samples annealed at 1000 °C. Fig. 5c shows a sample from the three-phase field [SbTi + T3 + L] whereas the sample shown in Fig. 5d represents the two-phase equilibrium [SbTi + L]; see also isothermal section in Fig. 4. The samples shown in Figs. 5e, f were used to localize the tie-line which separates the three-phase field [Sn_5Ti_6 + $Sb_{8-y}Ti_{11-x}$ + L] from the two-phase field [$Sb_{8-y}Ti_{11-x}$ + L]; see also Fig. 4.

Phase relations for Ti-contents between 62.5 and 75 at.% could only be determined at 1000°C. Despite extensive and multiple attempts (extension of the annealing times or further annealing cycles of powdered and cold pressed samples), a thermodynamic equilibrium was not achieved at lower temperatures due to insufficient diffusion at temperatures far below the liquidus. Hence, the corresponding phase triangulation at 1000 °C was transferred to both isothermal sections at low temperatures and adapted in consistency with the accepted binary systems; these equilibria are shown as dashed tie-lines. It has to be noticed that phase equilibria at Ti contents above 75 at.% could be established at 600 °C and 800 °C although the melting regime is even higher. We suppose the reason is that in Ti-rich samples the equilibrium phases arrive directly from primary crystallization whereas at Ti-contents between 62.5 and 75 at.% several phases need to be formed first at the respective annealing temperatures.

Pronounced solid solubility of the respective third element was observed for all binary compounds at all investigated temperatures, with the exception of SbTi. Homogeneity ranges run parallel to the Sb-Sn binary which suggests an interchange of Sb and Sn. The binary phases $SbTi_3$

and $SnTi_3$ show, beside a notable solubility of Sn or Sb respectively, also an extension of the homogeneity range towards the Ti-rich side. A fairly larger ternary solubility of Sn_3Ti_5 was found, which dissolves up to approx. 25 at.% Sb almost independently of temperature. The binary solubility of Sn_3Ti_5 towards the Ti-poor side (compare chapter 4.1.) extends into the ternary system and narrows slightly with raising Sb-content. A very high solubility of Sn in $Ti_{11-x}Sb_{8-y}$ up to around 30 at.% was found at all temperatures.

The compound T3 is nearly stoichiometric. All other three ternary phases show significant homogeneity ranges based on a Sb/Sn interchange. The stability field of T1 enlarges to more than 30 at.%, from around 18 to 49 at.% Sb with almost constant ~34 at.% Ti and the respective Sn concentration, at 600 °C. The solubility range of T2 and T4 is approx. 5 at.% at all three temperatures; however, T4 is formed only at 600 °C. In addition, a small enhancement of the Ti-content along with the substitution of Sn by Sb can be observed for T2.

4.2.1. Ti-rich corner (62.5-100 at.% Ti):

In the Ti-rich corner seven three-phase equilibria at 1000 °C occur (Fig. 4). Our experiments confirmed six of them directly, however, [Sb_3Ti_5 + Sn_3Ti_5 + T2] was estimated in consistency with the others, but could not be explicitly verified by our experiments.

At 600 °C and 800 °C phase analyses yielded the three-phase equilibrium [(Ti) + $SbTi_3$ + $SnTi_3$] together with the corresponding two-phase equilibria on either side (see Figs. 2 and 3). In the concentration range 62.5-75 at.-% Ti, the phase equilibria had to be adapted from the phase analyses at 1000 °C as discussed above (dashed lines).

At all investigated temperatures, the Ti-rich area of the phase diagram is dominated by the ternary compound T2 ($(Sb_xSn_{1-x})_{3-y}Ti_{5+y}$), which is part of six adjacent three-phase equilibria. Titanium shows a significant solid solubility of Sb and Sn at all temperatures.

4.2.2. Isotherms below 62.5 at.% Ti:

This part of the phase diagram is characterized by the appearance of in total three ternary phases (T1, T3 and T4), forming respective phase equilibria at distinct temperatures. In contrast to T2, which occurs in the entire investigated temperature range, T1 and T4 were observed only at lower, but T3 at higher temperatures. Below 33 at.% Ti, (Sb) is the only solid equilibrium phase occurring at 600 °C, while at the higher temperatures this part of the ternary system is fully

liquid. Therefore, the (Sb, Sn)-rich side of the ternary system is dominated by the liquid phase, which is involved in almost all phase equilibria.

The isothermal section at 1000 °C is dominated by three relatively wide two-phase fields ($Sb_{8-y}Ti_{11-x}$ + L, SbTi + L and Sb_2Ti + L). Since the equilibrium liquidus concentrations could not be determined experimentally, phase boundaries of the respective phase equilibria were constructed based on a large number of samples synthesized in this region (see chapter 4.2.). Eight three-phase fields are located in this composition range, seven of them were confirmed experimentally. [$Sb_{8-y}Ti_{11-x}$ + SbTi + T3] was added in consistency with phase rules. The ternary compound T3 appears in the isotherm at 1000 °C and is part of the three phase triangles [$Sb_{8-y}Ti_{11-x}$ + SbTi + T3], [$Sb_{8-y}Ti_{11-x}$ + T3 + L] and [SbTi + T3 + L].

In the isothermal section at 800 °C nine three-phase fields were confirmed by experiments during our studies; see Fig. 3. Compared to the isotherm at 1000 °C it mainly differs in the occurrence of a second ternary compound T1 and the absence of Sb_8Ti_5, which is only stable from 950 °C to 1092 °C in the binary system Sb-Ti [36]. The nearly stoichiometric compound T3 still exits at 800 °C but with a slightly higher Sn content compared to this at 1000 °C. A homogeneity range of around 5 at.% from 44 to 49 at.% Sb, with constant Ti content of ≈ 33-34 at.%, was observed for T1. It has to be noted that the composition range of T1 at this temperature deviates strongly from the assigned formula SbSnTi [1, 48]. The authors of [48] synthesized stoichiometric and nearly stoichiometric samples of TiSnSb from the elements at 850 °C. They [48] claimed phase purity with a very small or even negligible homogeneity range. This is in contradiction with our result. It has to be mentioned that no detailed information to the sample preparation is provided.

Phase relations at 600 °C again strongly differ from those at 800 °C and 1000 °C. While the ternary phase T3 is absent at this temperature, an additional ternary phase T4 arise. Both ternary phases, T4 as well as T1 show significant homogeneity ranges. The one of T4 is 12.5-17.5 at.% Sb at a constant Ti content of ≈ 44-45 at.%, whereas the one of T1 is much larger and extends from 21 to 49 at.% Sb with a constant Ti content of ≈ 33-34 at.%. This range also covers stoichiometric SbSnTi. Eleven three-phase fields were found, out of which eight are based on experimental results from equilibrium samples; [(Sb) + Sb_2Ti + L], [$Sb_{8-y}Ti_{11-x}$ + Sn_3Ti_5 + Sn_5Ti_6]

and [$Sb_{8-y}Ti_{11-x}$ + Sn_3Ti_5 + Sb_3Ti_5] were estimated in consistency with other results and phase rules.

Comparing the stability range of T1 at 600 °C and 800 °C strong narrowing and shift towards higher Sb-contents was observed so that the stoichiometric composition SnSbTi is not anymore covered. This phase does not exist at 1000 °C and seems to decompose at a concentration far from the stoichiometric one. A similar behavior is described for the binary Sb_xSn_{1-x} phase, which shows extended non-stoichiometry and a peritectic reaction at the highest possible Sb content [13].

4.3. Ternary crystal structures in the Sb-Sn-Ti system

During this study four ternary phases were observed and listed in Table 5: T1 (SbSnTi) [1, 48] and T2, $(Sb_xSn_{1-x})_{3-y}Ti_{5+y}$ (mentioned as Sb_2SnTi_5 in [60]) were already known from the literature, the latter was only forecasted based on ab-initio calculations. The existence of two new ternary compounds T3, Sb_4SnTi_5 and T4, $Sb_xSn_{19-x}Ti_{15}$, was at first indicated by powder X-ray patterns of several samples showing additional diffraction peaks at comparable angular positions that could not be allocated to any known crystal structure. Single crystal X-ray studies were carried out to identify and provide experimental structural information for $Sb_xSn_{19-x}Ti_{15}$ (T4), $(Sb_xSn_{1-x})_{3-y}Ti_{5+y}$ (T2) and Sb_4SnTi_5 (T3).

The binary phase Sn_3Ti_5 (see chapter 4.1.) shows a homogeneity range of approx. 2 at.% in the binary towards the Sn-rich side; additionally it is able to dissolve up to 25 at.% Sb. From powder patterns of ternary alloys containing this solubility phase, it was obvious that there are some significant differences in the relative peak intensities depending on the Ti content. Therefore, SCXRD investigations of two crystals taken from ternary samples with respective compositions were performed. The chemical compositions determined by EDX measurements are: $Sb_{18.3}Sn_{20}Ti_{61.7}$ (annealed at 800 °C) and $Sb_{8.5}Sn_{32}Ti_{59.5}$ (annealed at 600 °C). The results of all single crystal structure refinements are summarized in Tables 1 and 2.

4.3.1. Crystal structure determination and refinements

Sb_4SnTi_5, designated here as T3, shows an incommensurately modulated crystal structure. Despite many attempts, no proper single crystal for a complete structure solution could be found until now. Preliminary data from intergrown crystal species suggest an average

orthorhombic unit cell with the lattice parameters a = 5.64 Å, b = 17.54 Å, c = 4.48 Å. Satellites pointing at incommensurability were observed, but due to bespoke intergrowth, the q-vectors could not yet be unambiguously determined. Furthermore, intergrowth in the investigated crystals caused reflexes to overlap in such a way that definition of the integration boundary for the determination of the peak intensity was not possible without introduction of an arbitrary bias.

$Sb_xSn_{19-x}Ti_{15}$ ($x \sim 4.75$), designated here as T4, crystallizes in a new structure type. The cell metric is cubic, the Laue symmetry is $m\bar{3}$ and the extinction symbol is *P*---; reflection statistics suggested centrosymmetry. Space group $Pm\bar{3}$ (no. 200) is evident from structure refinements. The three crystallographically different positions of the atoms *M* = (Sb and/or Sn) were obtained by direct methods. Successive Fourier and difference Fourier summations revealed the three remaining atom sites. Well-balanced displacement parameters suggest an occupation of the sites 1(*b*), 6(*g*), and 8(*i*) by Ti atoms (i.e., 15 Ti atoms per unit cell). In analogy, the sites 1(*a*), 6(*h*) and 12(*j*) are occupied by *M* atoms (i.e., 19 *M* atoms per unit cell); see also Table 2.

The EDX analysis of the respective phase of the sample, of which the crystal for the structure determination came from, showed the atomic ratio of Ti:Sb:Sn is 44:14:42, see Table 2s, sample 15 in the supplementary material. According to this composition and based on the assumption of 15 Ti atoms per unit cell, ≈ 19 *M* atoms should be present per unit cell which well confirms the Ti/(Sb,Sn) ratio gained from the crystal structure refinement. The Sb:Sn ratio of 4.75:14.25 gives no hint for a preferred occupation of the sites 1(*a*), 6(*e*) and 12(*j*) resulting in a (partial) order of the Sn and Sb atoms. Consequently, a mixed occupation of the three *M* sites is assumed. Partial order or preferred occupation of any sites by either Sb or Sn atoms might be present but was not proved by conventional X-ray techniques due to the similar scattering power of Sb and Sn atoms.

$(Sb_xSn_{1-x})_{3-y}Ti_{5+y}$ ($0.44 \leq x \leq 0.61$; $0.11 \leq y \leq 0.20$), designated here as T2, crystallizes in the structure type W_5Si_3 [61]. The corresponding atomic coordinates of W_5Si_3 served in the starting set of structure refinements; it was assumed that the Ti and *M* atoms (*M* = Sb, Sn) occupy the two W sites and the two Si sites, respectively. Order of atoms occupying the two *M* sites of the structure type W_5Si_3 results in the Nb_5Sn_2Si-type structure (ternary-$D8_m$ type). In connection with a study on electronic structures of ternary compounds, with the composition Ti_5Sb_2X (X = Al, Ga, In, Si, Ge, Sn) crystallizing in the Nb_5Sn_2Si-type structure, Colinet and Tedenac [60] performed ab-inito calculations also for Sb_2SnTi_5. The ratio Sb:Sn = 2:1 considered for the

theoretical calculations accords with an ordered occupation of the sites 8(*h*) (*M*2) and 4(*a*) (*M*1) with Sb and Sn atoms, respectively. The crystal used for the present experimental investigations, however, deviates from the end-member composition Sb_2SnTi_5. The chemical EDX-analysis of the utilized phase, of a sample with the composition $Sb_{20}Sn_{16.7}Ti_{63.3}$ annealed at 1000 °C, gave the composition $Sb_{20.4}Sn_{15.8}Ti_{63.8}$ with a ratio Sb:Sn = 1.29. A widely varying Sb:Sn ratio from 0.82 to 1.29 was observed at 1000 °C, but an extension of the phase field to a ratio Sb:Sn = 2:1 was never monitored. Consequently, the compound under investigation represents a ternary phase with a certain solid solubility for which a mixed occupation of at least the *M*2 site by Sb and Sn atoms is required. Due to the similar scattering power of the Sb and Sn atoms using conventional X-ray sources, it is questionable whether the *M*1 site is occupied by Sn atoms only (as in stoichiometric Sb_2SnTi_5) or by Sb+Sn atoms in variable ratios. A phase with the stoichiometric composition Sb_2SnTi_5 as assumed in [60] could not be verified during our investigations (see chaper 4.2). Some kind of mixed occupation of the *M* site(s) seems to stabilize the compound.

Conspicuous large isotropic displacement parameters of the *M* sites, as compared to those of the Ti atoms, suggested a partial substitution of Sb/Sn by Ti atoms or even the formation of vacancies. Accordingly, a partial substitution by Ti atoms with varying ratios of *M*:Ti was allowed at the *M*-sites sites 4(*a*) and 8(*h*). This reduced the R values significantly and resulted in well-balanced displacement parameters: considering Ti atoms at the *M* sites reduced *R*1 from 0.033/0.028 for all/observed reflections to 0.023/0.018 and *wR*2 from 0.069 to 0.038. Thus, the additional substitution of the *M* sites by Ti atoms was proofed by X-ray investigation if full occupation for all four sites is expected. The Ti substitution (or facultative vacancies) at the 8(*h*) site is very low, but it is highly significant at the 4(*a*) site. The chemical composition resulting from structure refinements based on the assumption that the sites 4(*a*) and 8(*h*) have no vacancies is $(Sb,Sn)_{2.84}Ti_{5.16}$, the given structural formula is $(Sb_xSn_{1-x})_{3-y}Ti_{5+y}$ with y = 0.16. The Ti:M (Sb, Sn) ratio is 1.82 which well compares to this of 1.76 from the EDX measurements of the phase whereof the single crystal has been depicted. Our experimental results presented here are in excellent agreement with the lattice parameters and atomic coordinates theoretically calculated in [60], however, the site occupation differs.

$(Sb_xSn_{1-x})_{3+y}Ti_5$ ($0 \le x \le 0.67$; $0 \le y \le 0.4$) represents the ternary solubility of the binary phase Sn_3Ti_5 which also shows a binary solubility towards the Sn-rich side. From powder patterns of ternary alloys containing this phase at various concentrations isotypy with the earlier

described compound Sn_3Ti_5 was assumed (structure type $D8_8$, Mn_5Si_3, Pearson symbol *hP*16; [62, 63]). The powder patterns taken of phases with distinct compositions along this solubility range roughly confirmed the structure type Mn_5Si_3; however, minor but significant differences in the intensity distribution are evident.

At first, the structure refinement of a single crystal from an equilibrium phase with the nominal composition $Sb_{8.5}Sn_{32}Ti_{59.5}$ = $(Sb_{0.21}Sn_{0.79})_{3.40}Ti_5$ at the Ti-poor side of the ternary solubility (see sample 7 in Table 2s in supplementary material) was done. It was started with the structure model given by Nowotny et al. [63] with space group symmetry $P6_3/mcm$ and Ti atoms at 6(*g*) (*x* = 0.240) and 4(*d*) but Sb atoms at 6(*g*) (*x* = 0.615), labeled as Ti1, Ti2 and M1. As mentioned above, site occupation with Sn or Sb atoms, respectively, were not considered due to the only small difference in the scattering power. Therefore, these positions are labeled *M* although the scattering function of Sb is arbitrarily chosen for the refinements. Interestingly, the difference Fourier summation showed an additional maximum for the residual electron density at the origin of the unit cell (0, 0, 0). This new position with the Wyckoff letter 2(***b***) was labelled *M*2 and included with the scattering function of Sb but with a variable site occupation factor (s.o.f.). Furthermore, the two Ti sites Ti1 and Ti2 exhibited a small but significant higher scattering power as compared to that expected for an occupation with solely Ti atoms. We assume a partial occupation with Sb or Sn atoms but the trial to refine the ratio of the scattering functions Sb:Ti under assumption of full occupation failed. Therefore, only the site occupation factor was allowed to vary during the final refinement cycles. The resulting s.o.f. > 1.0 is physically meaningless, it reflects the average electron density only.

Another single crystal of an equilibrium phase with the composition $Sb_{18.3}Sn_{20}Ti_{61.7}$ = $(Sb_{0.48}Sn_{0.52})_{3.10}Ti_5$ at the Ti-rich side of the ternary solubility was investigated by SCXRD. The structure refinement gave within limits of error a full occupation of the Ti1 and Ti2 positions solely with Ti atoms and only minor scattering power for the additional site *M*2.

A recalculation of the compositions of the two compounds according to the refined structure model (Table 2) gives $M_{3.44}Ti_5$ and $M_{3.12}Ti_5$, respectively, which is in quite good agreement with the chemical analysis. In a strict sense, both compounds are not isotypic with the structure type Mn_5Si_3, as an additional atom position 2(*b*) was introduced.

4.3.2. Stereochemistry

$Sb_xSn_{19-x}Ti_{15}$, T4: The six crystallographically different coordination figures in the crystal structure of T4 are shown in Fig. 6. The *M*1 atom is coordinated by twelve *M*3 atoms forming a highly symmetric icosahedron with point symmetry $m\bar{3}$ and equidistant *M*1—*M*3 bond distances (Fig. 6a). This $M1M3_{12}$ polyhedron represents the largest coordination figure found in the investigated compounds. A second quite regular shaped coordination figure shown in Fig. 6b. is a hexa-capped cube formed by eight Ti3 and six *M*2 atoms which surround the Ti1 atom. It should be mentioned that the bond lengths to the *M*2 atoms are shorter than those to the Ti3 atoms; thus, the coordination figure could also be described as an octa-capped octahedron. For all other atoms, the coordination is not clear-cut. Moreover, the coordination figures are irregular and partly one-sided despite of their high point symmetries. They are shown in Fig. 6 c-f.

$(Sb_xSn_{1-x})_{3-y}Ti_{5+y}$, T2: The four crystallographically different coordination figures in the crystal structure of T2 are shown in Fig. 7. The *M*1 atom is coordinated by a tetragonal antiprism formed by eight Ti2 atoms which is capped by *M*1 atoms (Fig. 7a). The hexagonal antiprism around the Ti1 atom is formed by two *M*2 and four Ti2 atoms at each side (Fig. 7b); it is capped by Ti1 atoms. The coordination of the M2 and the Ti2 atoms are both related to a distorted icosahedrons (Figs. 7c-d). The coordination figures of the crystal structure of T2 are described in more details in [60].

$(Sb_{0.21}Sn_{0.79})_{3.40}Ti_5$ and $(Sb_{0.48}Sn_{0.52})_{3.10}Ti_5$: As expected, filling of the channels of the Mn_5Si_3-type structure along [001] as indicated in Fig. 8 influences the cell metric where *a* is less effected as compared to *c*. The cell parameters *a* and *c* increase from $M_{3.10}Ti_5$ to $M_{3.40}Ti_5$ by 1.40 and 2.14 %, respectively. Most atoms, i.e., Ti2 and *M*1 at 6(*g*), are located in *z* = 1/4 and 3/4; they stabilize the crystal structure parallel (0001). Only the atoms Ti2, 4(*d*), and *M*2, 2(*b*) are in between. Therefore, the crystal structure is less stiff and rather flexible along [001] than in (0001). Most striking is the variation of the bond distance Ti1—*M*2 in these two samples (2.4129 and 2.5772 Å). In any case, the latter is still short for a Ti—(Sb,Sn) bond. As a consequence, the displacement parameter of the Ti1 atom in $M_{3.40}Ti_5$ is large and shows a conspicuous anisotropy (principal mean square atomic displacements are 0.040, 0.016, and 0.010 Å²) going along with

the by far largest peak in the difference Fourier summation (at 0.196, 0, 1/4, i.e., 0.56 Å off the Ti1 atom at 0.246, 0, 1/4).

The four crystallographically different coordination figures in the crystal structure of the two compounds are shown in Fig. 9. Four Ti2 and two Ti1 atoms form a trigonal prism around the *M2* atom (Fig. 9a); seven further ligands (two *M1*, two *M*2 and three Ti1 atoms) are arranged in a quite regular planar seven-folded equatorial ring. Six *M1* and two *M2* atoms surround the *M*2 atom in form of a distorted tetragonal prism; it is capped by six Ti1 atoms (Fig. 9b). The Ti1 atom is coordinated in form of a pentagonal prism formed by Ti atoms; the top and bottom faces are capped by *M*1 atoms, the prism faces by three *M*1 and two *M2* atoms, respectively (Fig. 9c). The Ti2 atom is surrounded by an approximate hexagonal antiprism formed by *M*1and Ti1 atoms; the top and bottom faces are capped by Ti2 atoms (Fig. 9d).

4.3.3. Topology

Structural relations between T4 ($Sb_xSn_{19-x}Ti_{15}$), T2 ($(Sb_xSn_{1-x})_{3-y}Ti_{5+y}$) and T1 (SbSnTi) [1, 48] are evident. The crystal structure of the cubic compound T4 forms a three-dimensional network. $M1M3_{12}$ clusters are linked among each other *via M*2 and Ti atoms, see Fig. 10a. Considering the connection of the coordination figures around the *M*2 and Ti1 atoms, chains parallel to <100>, i.e. in (½ ½ *z*) etc., are formed (Fig. 11a); they intersect each other in (½ ½ ½).

In the atomic arrangement of T2 two different chains of M1 and Ti1 atoms run parallel to [001], see Fig. 10b. Eight Ti2 atoms coordinate the *M*1 atoms forming a tetragonal antiprism. They are connected via their two square faces (Fig. 11b). Eight Ti2 and four *M*2 atoms form a hexagonal antiprism around the Ti1 atoms; they are linked via their basal and top faces to one-dimensional columns (Fig. 11c). Both columns run parallel to [001]. This building unit is in analogue to that found in T1, SbSnTi, but there the Sb_4Sn_4 antiprisms are centered by Ti atoms.

A general feature found in the crystal structures of compounds in the Sb–Sn–Ti ternary system are channels. In the title compound $Sb_xSn_{19-x}Ti_{15}$, T4, the channels run along (0.5 0.5 *z*). They are filled by Ti1 and M2 atoms; their coordination figures share opposite $(Ti3)_4$ squares (Fig. 11a). In $(Sb_xSn_{1-x})_{3-y}Ti_{5+y}$, T2, occur two crystallographically different channels. One is running along (0 0 *z*) and (½ ½ z); it is solely filled by *M*1 atoms (Fig. 11b). The respective coordination figures are linked by opposite $(Ti2)_4$ squares. The second channel along (½ 0 *z*) is filled by Ti1 atoms which are linked by hexagons formed by *M*2 and Ti2 atoms (Fig. 11c). In $(Sb_xSn_{1-x})_{3-y}Ti_5$ channels along (⅓ ⅔ *z*) and (0 0 *z*) are filled by *M*2 and Ti2 atoms, respectively (Fig. 11d, e); in both cases the coordination figures are linked via opposite hexagons.

5. Conclusion

Three isothermal sections at 600 °C, 800 °C and 1000 °C in the system Sb-Sn-Ti were studied; a large number of alloys were analyzed using powder X-ray diffraction (PXRD), light optical microscopy (LOM) and scanning electron microscopy (SEM/EDX). Single crystals were depicted from selected samples and analyzed in terms of single X-ray diffraction (SCXRD). In the investigated temperature range, all binary compounds in Sb-Sn-Ti except SbTi show a significant ternary solubility of the respective third element. As the homogeneity ranges generally run parallel to the Sb-Sn side, mixed occupation at the respective atomic sites might be assumed, although for the binary incommensurate compound SbSn the inclusion of Sb-layers in between Sb_3Sn_4 building blocks has been mentioned to be the predominant mechanism [13]. Nevertheless, the similar atomic radii, electronic structure and our results from SCXRD refinements support the possibility for the interchange of Sb and Sn atoms.

Four ternary compounds were found in the Sb-Sn-Ti system, from which T2 was only predicted from ab-initio calculations [60], whereas T3 and T4 have been reported for the first time. The crystal structure of T2 and T4 was experimentally determined the first time whereas that of T3 which is most probable incommensurate could not yet be clarified. T1, already well described in literature [1, 48], was found at 600 °C and 800 °C and is supposed to be stable down to room temperature since it can be synthesized by ball milling; in the scope of new anode materials for LIBs, stoichiometric T1 (SbSnTi) was the candidate phase for electrochemical lithiation investigations [2, 3]. T4 was only observed at 600 °C, and if stable down to room temperature, its role in the (de)lithiation process may have to be considered. On the other hand, T3 was observed only at 800°C and 1000 °C so that its lower stability limit must be between 600°C and 800°C.

Considering the possible application of Sb-Sn-Ti alloys as anode materials for LIBs, studies of the quaternary system Li-Sb-Sn-Ti and all involved ternary systems are highly indicated. For a profound understanding of lithiation pathways and mechanisms the knowledge of phases formed and their interactions are mandatory requirements. Therefore, we recently explored the ternary system Li-Sb-Sn [64]. In our current work we present the first extensive investigation of isotherms in the ternary system Sb-Sn-Ti. Further work, including additional isothermal sections, isopleth, liquidus projection and reaction schemes will be necessary to completely understand the phase relations of this system. Theoretical thermodynamic calculations as well as CALPHAD

assessments are required for a full description of the quaternary system Li-Sb-Sn-Ti which also provides electrochemical data, e.g. equilibrium voltages or thermal behavior.

Acknowledgments

The authors thank Dr. Stephan Puchegger from the Faculty of Physics, University of Vienna, for his support with SEM measurements. Special thanks go to Konstantin Moser, who performed some investigations during his Bachelor thesis as well as Yann Austernaud, from Université Grenoble Alpes, who performed some studies during his internship in our laboratory.

Figure captions:

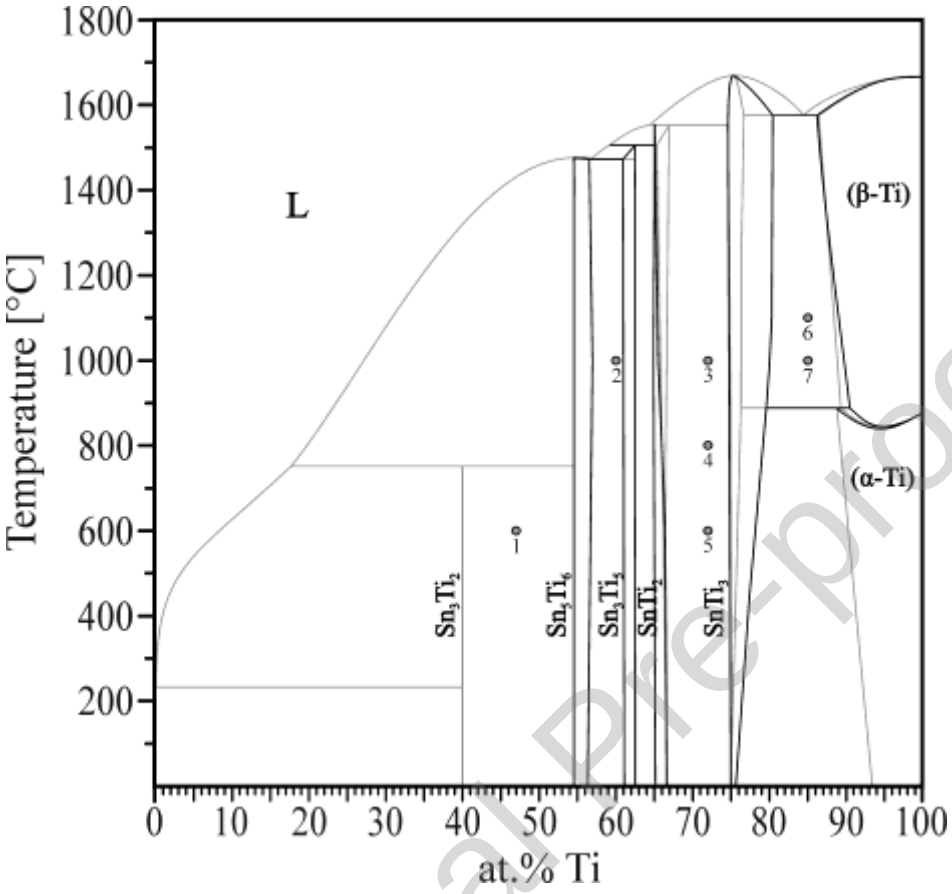

Figure 1: Sn-Ti system calculated by Wang et al. [44] is redrawn in grey; alterations according to our studies are shown in black. Annealed samples are indicated as filled circles.

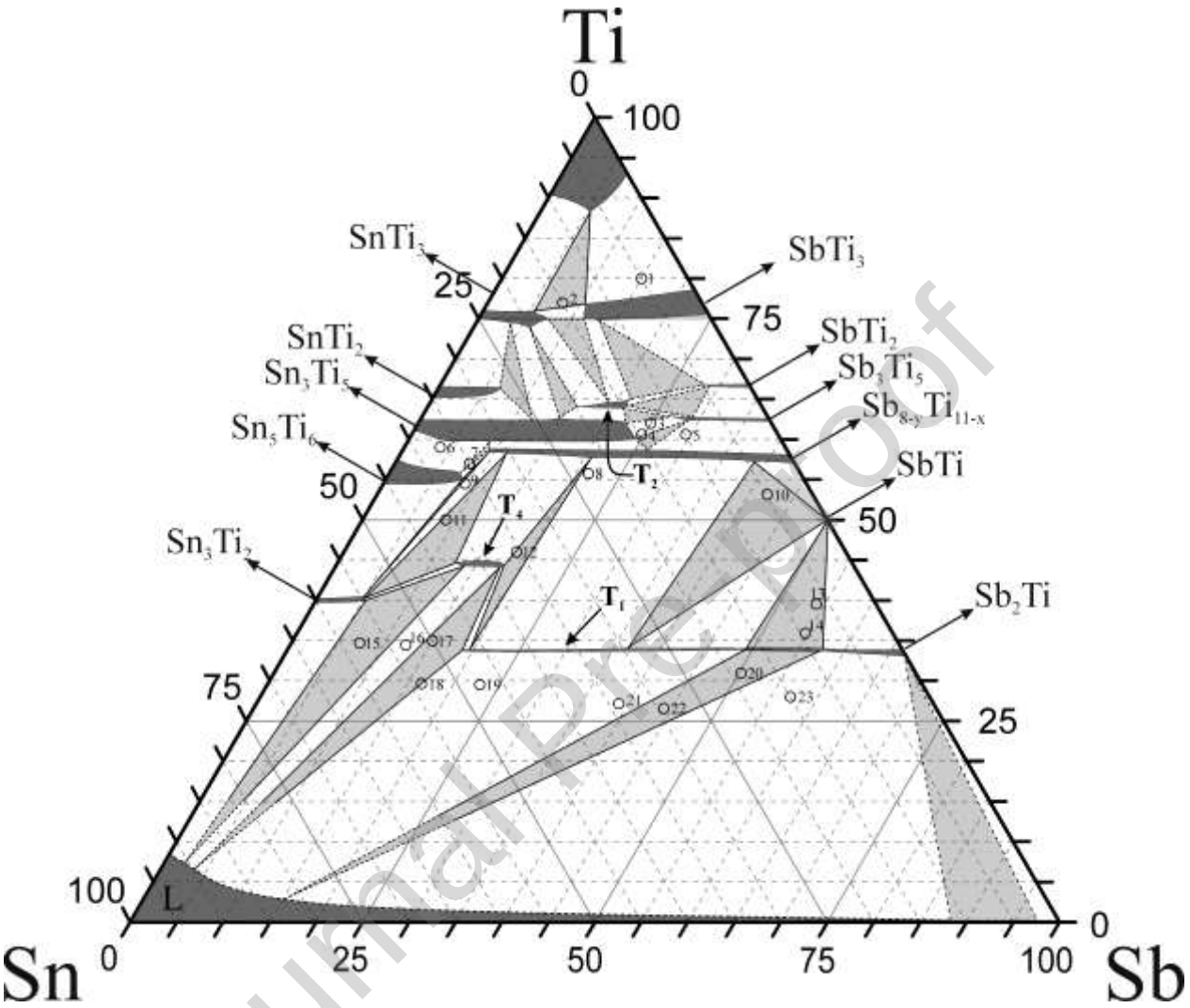

Figure 2: Isothermal section of the ternary system Sb-Sn-Ti at 600 °C with annealed samples, indicated as unfilled circles. Estimated phase equilibria are drawn with dashed lines. Single-, two- and three-phase equilibria are drawn in dark-greys, white and light grey, respectively.

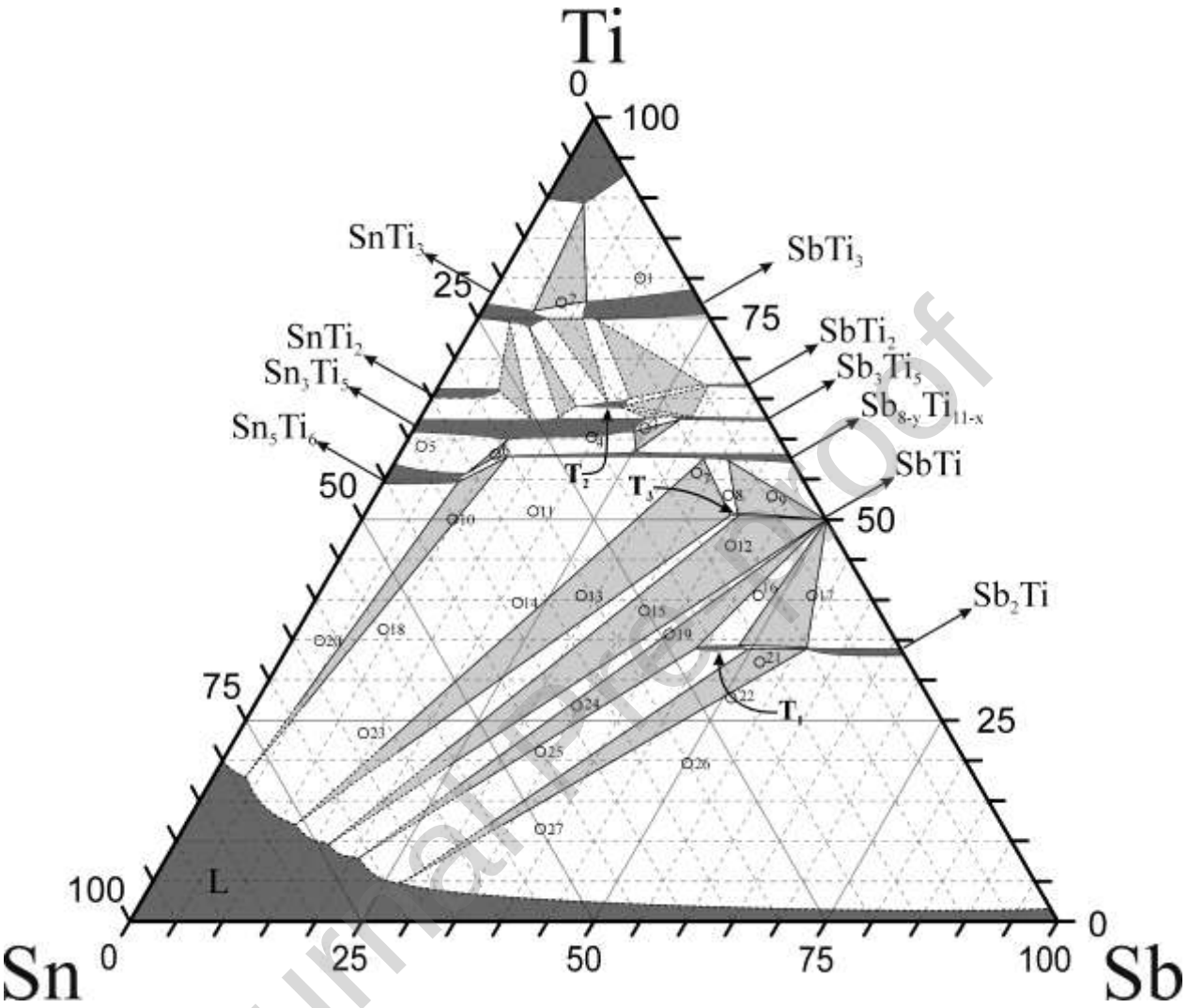

Figure 3: Isothermal section of the ternary system Sb-Sn-Ti at 800 °C with annealed samples, indicated as unfilled circles. Estimated phase equilibria are drawn with dashed lines. Single-, two- and three-phase equilibria are drawn in dark-greys, white and light grey, respectively.

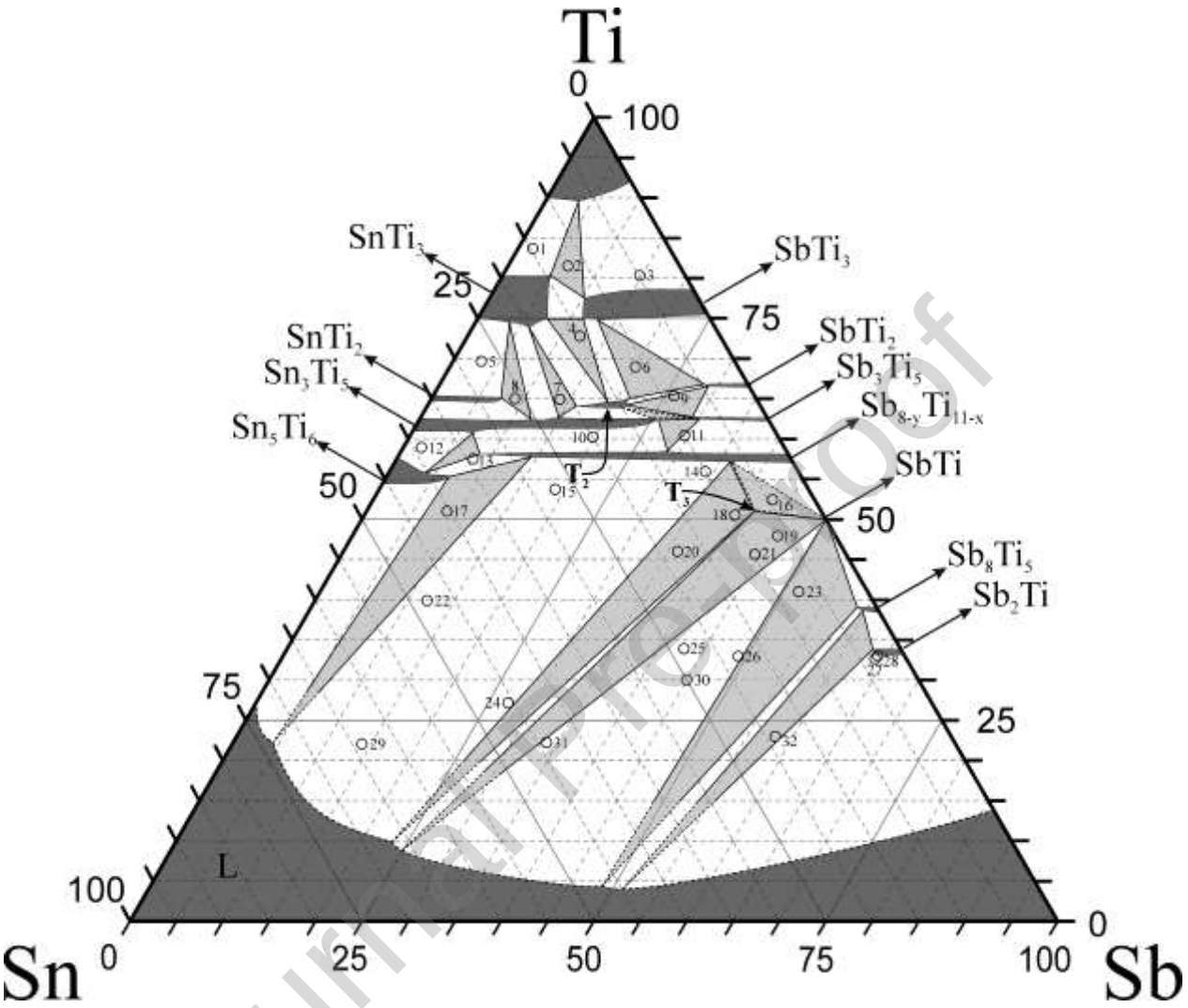

Figure 4: Isothermal section of the ternary system Sb-Sn-Ti at 1000 °C with annealed samples, indicated as unfilled circles. Estimated phase equilibria are drawn with dashed lines. Single-, two- and three-phase equilibria are drawn in dark-greys, white and light grey, respectively.

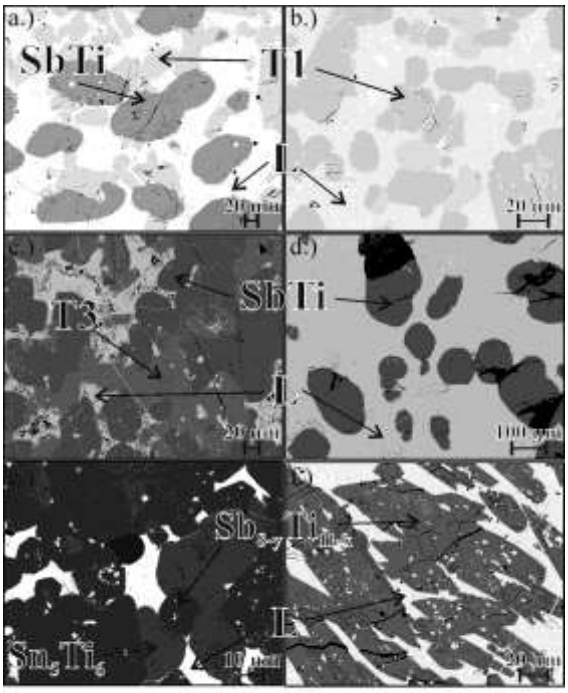

Figure 5: SEM-micrographs of representative annealed samples in the Sb-Sn-Ti system. Pairs of two- and three-phase samples are shown; a.) sample $Sb_{34.9}Sn_{38.3}Ti_{26.8}$ shows the three-phase equilibrium [SbTi + T1 + L] whereas b.) sample $Sb_{33.8}Sn_{45.1}Ti_{21.1}$ indicates the two-phase equilibrium [T1 + L], both annealed at 800 °C; c.) sample $Sb_{44.6}Sn_{9.8}Ti_{45.6}$ shows the three-phase equilibrium [SbTi + T3 + L], whereas d.) sample $Sb_{33.4}Sn_{44.1}Ti_{22.5}$ indicates the two-phase equilibrium [SbTi +L]; e.) sample $Sb_{8.8}Sn_{40.2}Ti_{51.0}$ shows the three-phase equilibrium [Sn_5Ti_6 + $Sb_{8-y}Ti_{11-x}$ +L] whereas f.) sample $Sb_{12}Sn_{48}Ti_{40}$ indicates the two-phase equilibrium [$Sb_{8-y}Ti_{11-x}$ +L]. The last four samples were all annealed at 1000 °C.

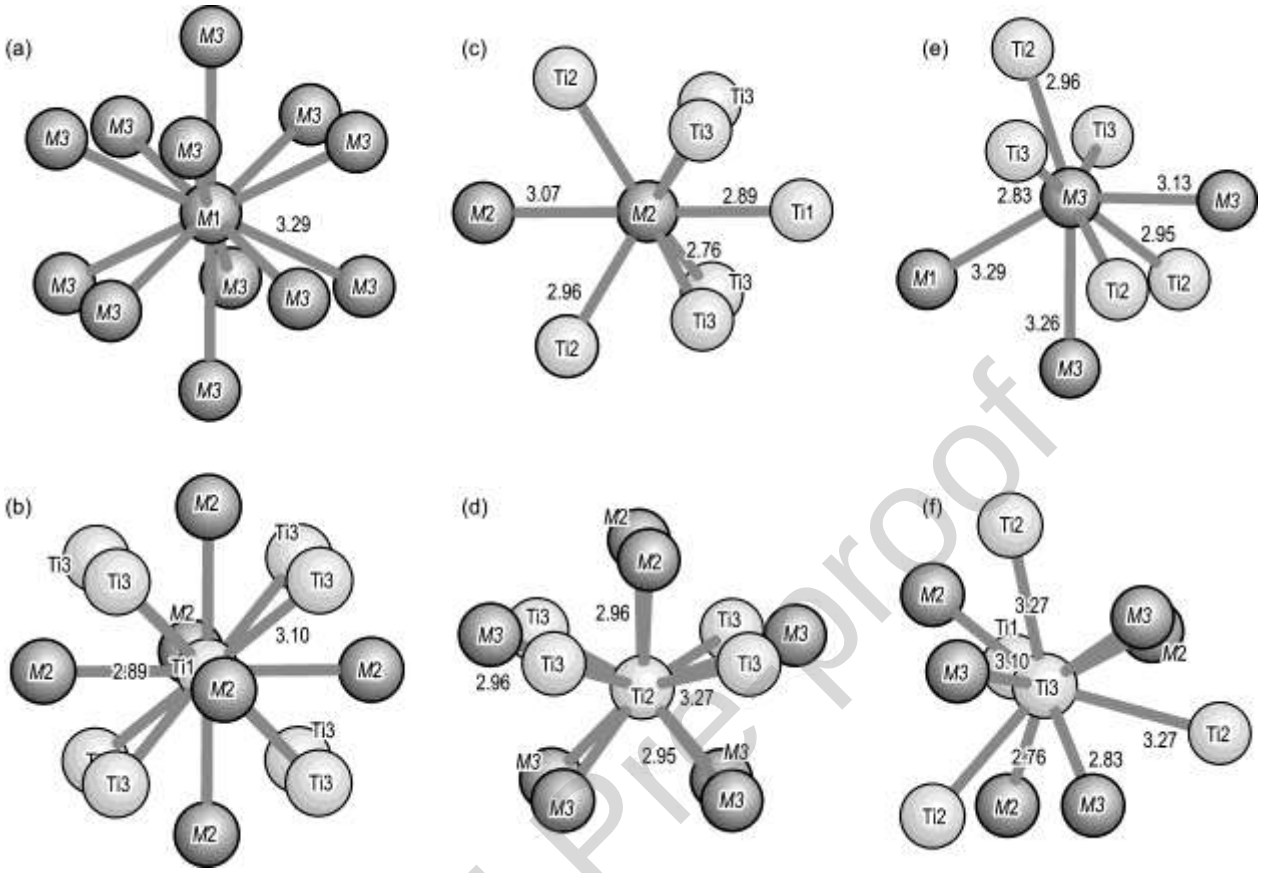

Figure 6: The coordination figures in $Sb_xSn_{19-x}Ti_{15}$, T4: (a) the *M*1 atom, site symmetry $m\bar{3}$; (b) the *M*2 atom, site symmetry *mm*2; (c) the *M*3 atom, site symmetry *m*; (d) the Ti1 atom, site symmetry $m\bar{3}$; (e) the Ti2 atom, site symmetry *mm*2; (f) the Ti3 atom, site symmetry 3. Interatomic bond distances are given in Å.

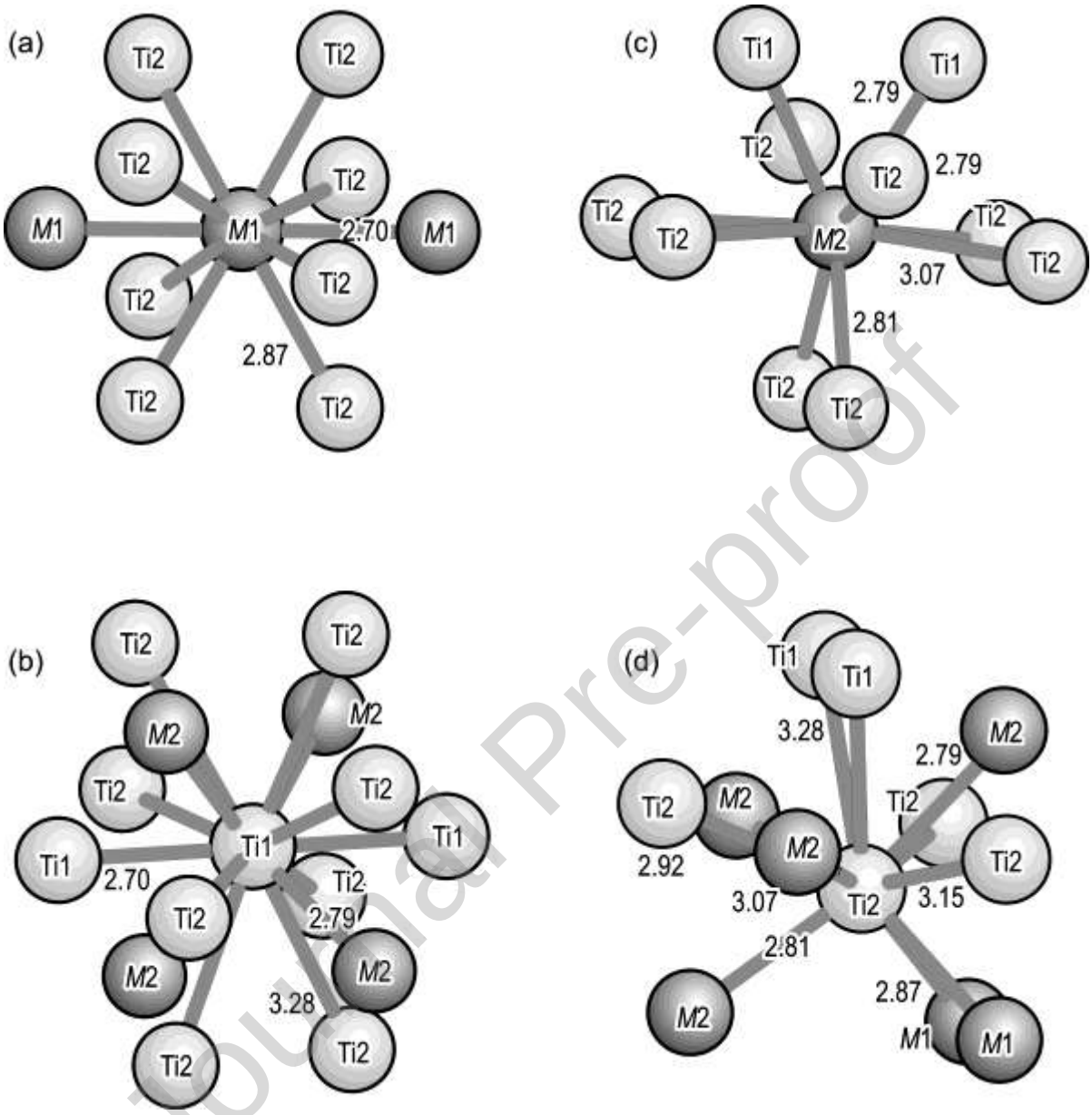

Figure 7: The coordination figures in $(Sb_xSn_{1-x})_{3-y}Ti_{5+y}$: (a) the *M*1 atom, site symmetry 422; (b) the *M*2 atom, site symmetry *mm*2; (c) the Ti1 atom, site symmetry $\bar{4}2m$; (d) the Ti2 atom, site symmetry *m*. Interatomic bond distances are given in Å.

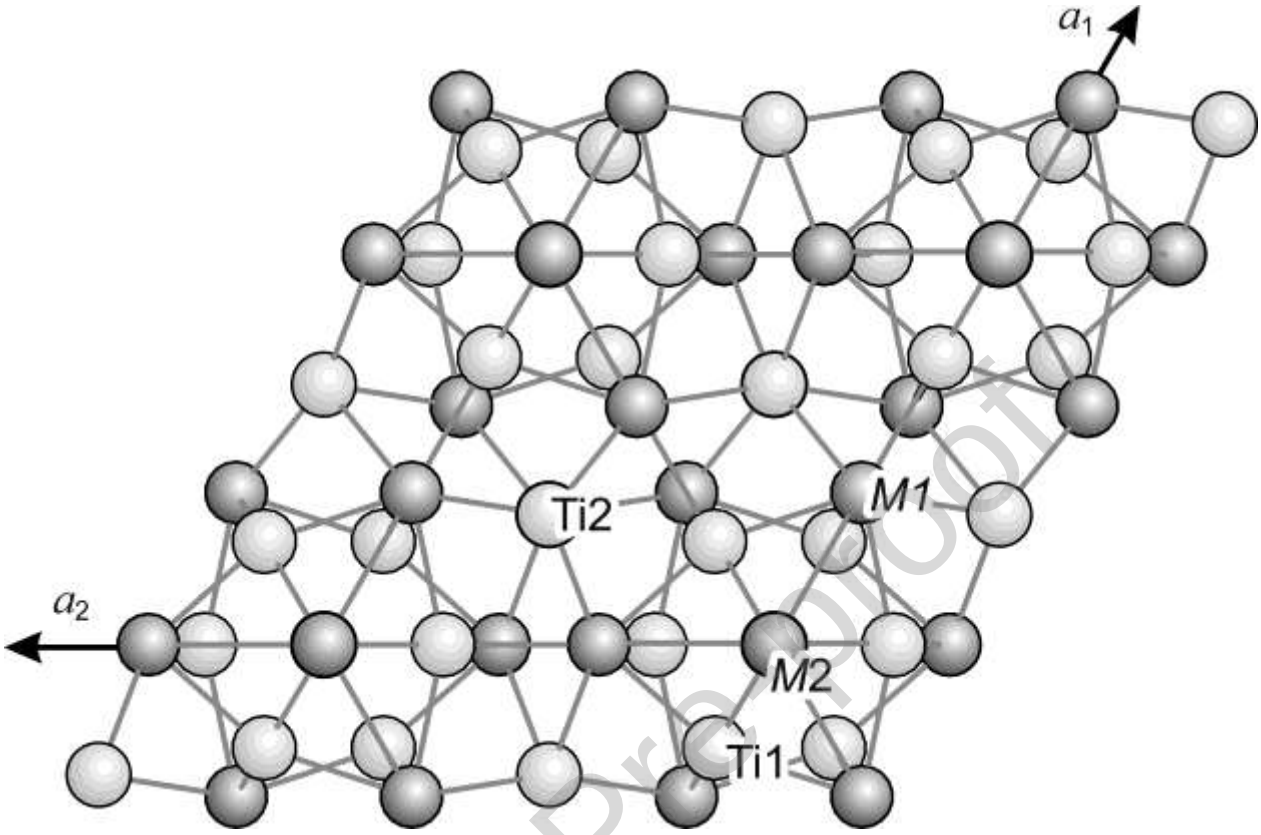

Figure 8: The crystal structure of $(Sb_{0.48}Sn_{0.52})_{3.10}Ti_5$ respectively $(Sb_{0.21}Sn_{0.79})_{3.40}Ti_5$ in a projection parallel to [001]. The difference between this crystal structure and the structure type Mn_5Si_3 is the additional occupation of the *M*2 position.

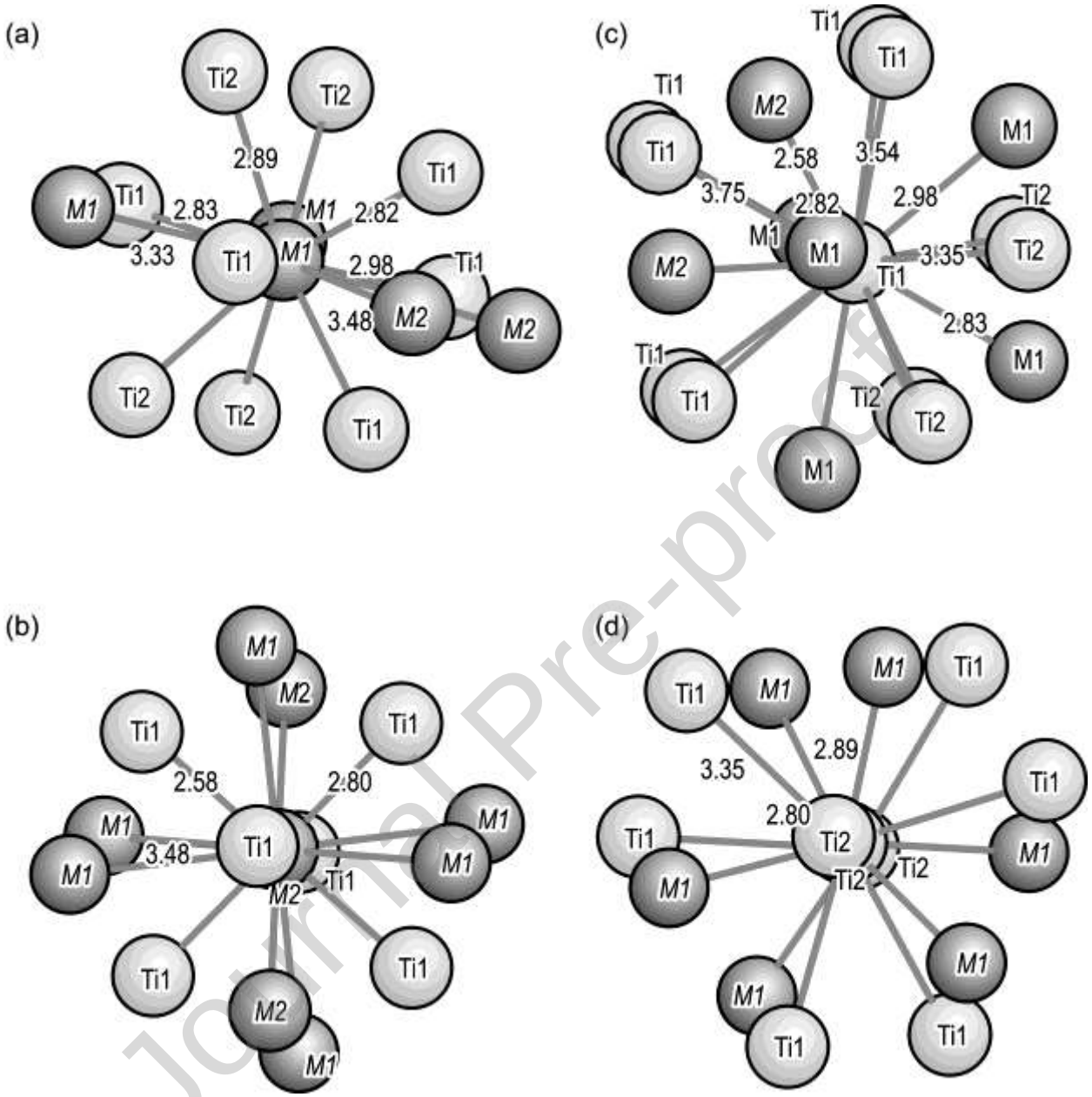

Figure 9: The coordination figures in $(Sb_{0.21}Sn_{0.79})_{3.40}Ti_5$: (a) the *M* atom, site symmetry *m*2*m*; (b) the *M*1 atom, site symmetry $\bar{3}$; (c) the Ti1 atom, site symmetry *m*2*m*; (d) the Ti2 atom, site symmetry 3.2. Interatomic bond distances are given in Å.

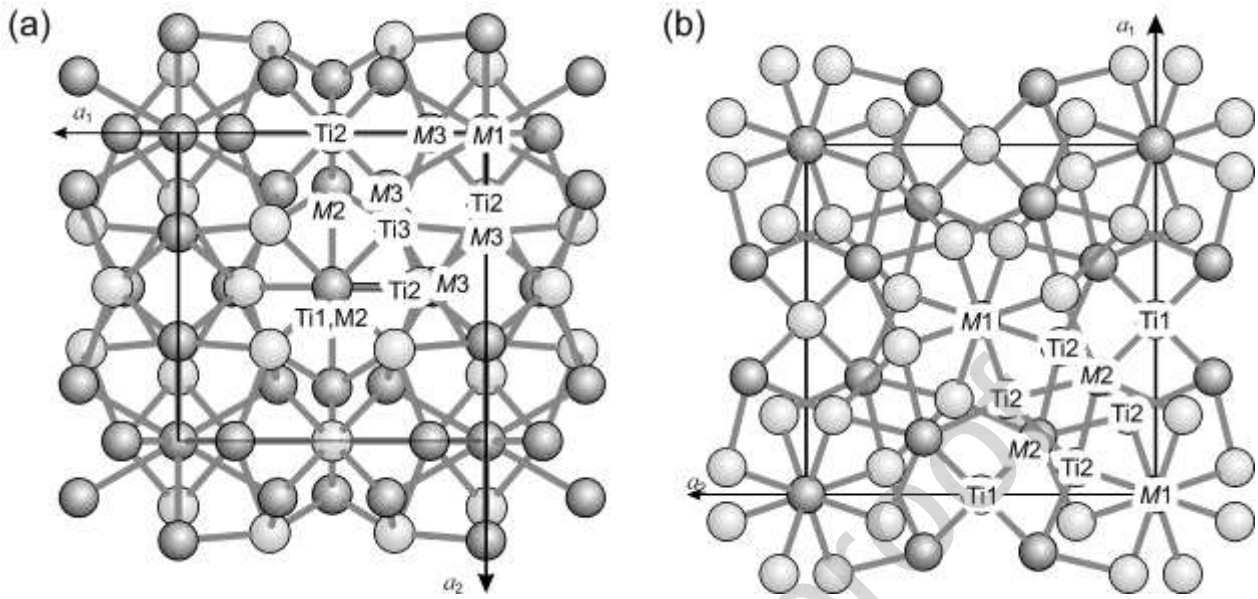

Figure 10: (a) The crystal structure of $Sb_xSn_{19-x}Ti_{15}$ in a projection parallel to [001]; (b) the crystal structure of $(Sb_xSn_{1-x})_{3-y}Ti_{5+y}$ in a projection parallel to [001].

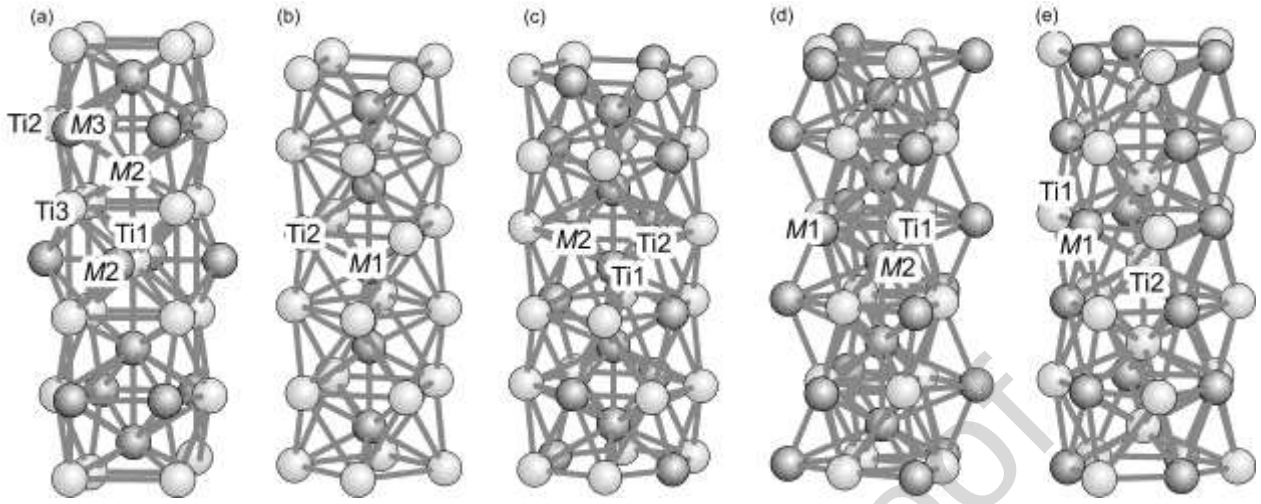

Figure 11: The chains formed in the two ternary compounds: (a) in $Sb_xSn_{19-x}Ti_{15}$ along (½ ½ z); in $(Sb_xSn_{1-x})_{3-y}Ti_{5+y}$ along (b) (0 0 *z*) and (c) (½ 0 *z*); and in the binary compound $(Sb_xSn_{1-x})_{3-y}Ti_5$ along (⅓ ⅔ *z*) (d) and (0 0 *z*) (e).

References

[1] B. Malaman, J. Steinmetz, 2 new ternaries with related structures - TiSnSb of $CuMg_2$ type and NbSnSb of $CuAl_2$ type, J. Less-Common. Met., 65 (1979) 285-288.
[2] M.T. Sougrati, J. Fullenwarth, A. Debenedetti, B. Fraisse, J.C. Jumas, L. Monconduit, TiSnSb a new efficient negative electrode for Li-ion batteries: mechanism investigations by operando-XRD and Mössbauer techniques, J. Mater. Chem., 21 (2011) 10069-10076.
[3] C. Marino, M.T. Sougrati, B. Gerke, R. Pottgen, H. Huo, M. Menetrier, C.P. Grey, L. Monconduit, Role of structure and interfaces in the performance of TiSnSb as an electrode for Li-Ion batteries, Chem. Mater., 24 (2012) 4735-4743.
[4] H.A. Wilhelm, C. Marino, A. Darwiche, L. Monconduit, B. Lestriez, Significant electrochemical performance improvement of TiSnSb as anode material for Li-ion batteries with composite electrode formulation and the use of VC and FEC electrolyte additives, Electrochem. Commun., 24 (2012) 89-92.
[5] W. Zhang, F. Ghamouss, A. Darwiche, L. Monconduit, D. Lemordant, R. Dedryvere, H. Martinez, Surface film formation on TiSnSb electrodes: Impact of electrolyte additives, J. Power Sources, 268 (2014) 645-657.
[6] H.A. Wilhelm, C. Marino, A. Darwiche, P. Soudan, M. Morcrette, L. Monconduit, B. Lestriez, Engineering study on TiSnSb-based composite negative electrode for Li-ion batteries, J. Power Sources, 274 (2015) 496-505.
[7] W. Zhang, F. Ghamouss, A. Mery, D. Lemordant, R. Dedryvere, L. Monconduit, H. Martinez, Improvement of the stability of TiSnSb anode under lithiation using SEI forming additives and room temperature ionic liquid/DMC mixed electrolyte, Electrochim. Acta, 170 (2015) 72-84.
[8] M. Fehse, A. Darwiche, M.T. Sougrati, E.M. Kelder, A.V. Chadwick, M. Alfredsson, L. Monconduit, L. Stievano, In-depth analysis of the conversion mechanism of TiSnSb vs Li by operando Triple-Edge X-ray absorption spectroscopy: a chemometric approach, Chem. Mater., 29 (2017) 10446-10454.
[9] L. Madec, G. Gachot, G. Coquil, H. Martinez, L. Monconduit, Toward efficient Li-ion cells at high temperatures: example of TiSnSb material, J. Power Sources, 391 (2018) 51-58.
[10] A. Beutl, D. Cupid, H. Flandorfer, The Li-Sb phase diagram part I: New experimental results, J. Alloy. Compd., 695 (2017) 1052-1060.
[11] D. Li, S. Fürtauer, H. Flandorfer, D.M. Cupid, Thermodynamic assessment and experimental investigation of the Li-Sn system, Calphad, 47 (2014) 181-195.
[12] C. Schmetterer, J. Polt, H. Flandorfer, The phase equilibria in the Sb-Sn system - Part I: Literature review, J. Alloy. Compd., 728 (2017) 497-505.
[13] C. Schmetterer, J. Polt, H. Flandorfer, The phase equilibria in the Sb-Sn system - Part II: Experimental results, J. Alloy. Compd., 743 (2018) 523-536.
[14] L. Noren, R.L. Withers, S. Schmid, F.J. Brink, V. Ting, Old friends in a new light: "SnSb" revisited, J. Solid State Chem., 179 (2006) 404-412.
[15] M. Hansen, K. Anderko, Constitution of binary alloys, 2 ed., McGraw-Hill, New York, 1958.
[16] A. Stegherr, A three-component system of tin-antimony-tellurium, Philips Res. Rep., (1969) 25-28.
[17] T.B. Massalski, H. Okamoto, Binary alloy phase diagrams, 2nd ed., ASM International, Materials Park, Ohio, 1990.
[18] S.W. Chen, C.C. Chen, W. Gierlotka, A.R. Zi, P.Y. Chen, H.J. Wu, Phase equilibria of the Sn-Sb binary system, J. Electron. Mater., 37 (2008) 992-1002.
[19] H. Okamoto, Sb-Sn (antimony-tin), J. Phase Equilib., 19 (1998) 292-292.
[20] B. Predel, W. Schwermann, Constitution and thermodynamics of antimony-tin system, J. I. Met., 99 (1971) 169-172.
[21] G. Borzone, S. Delsante, D. Li, R. Novakovic, New insights into phase equilibria of the Sb-Sn system, J. Phase Equilib. Diff., (2021).
[22] V.A. Lysenko, Thermodynamic reassessment of the Sb-Sn and In-Sb-Sn systems, J. Alloy. Compd., 776 (2019) 850-857.

[23] W. Gierlotka, On the binary Sb-Sn system: ab initio calculation and thermodynamic remodeling, J. Mater. Sci., 55 (2020) 347-357.
[24] H. Nowotny, J. Pesl, Untersuchungen im System Titan-Antimon, Monatsh. Chem. , 82 (1951) 336-343.
[25] H. Nowotny, R. Funk, J. Pesl, Kristallchemische Untersuchungen in den Systemen Mn-As, V-Sb, Ti-Sb, Monatsh. Chem., 82 (1951) 513-525.
[26] H. Auer-Welsbach, H. Nowotny, A. Kohl, Untersuchung reibungspyrophorer Ti-Legierungen; Ti_2Bi, ein neuer Strukturtyp, Monatsh. Chem., 89 (1958) 154-159.
[27] A. Kjekshus, F. Grønvold, J. Thorbjørnsen, On the phase relationships in the titanium-antimony system. The crystel structure of Ti_3Sb, Acta Chem. Scand., 16 (1962) 1493-1510.
[28] A.Y. Kozlov, V.V. Pavlyuk, New ternary antimonides Ti_5XSb_2 with W_5Si_3 structure type, Intermetallics, 11 (2003) 237-239.
[29] R. Berger, Structure refinement of Ti_5Sb_3 from single-crystal data, Acta Chem. Scand., 31a (1977) 889-890.
[30] J. Murray, Phase diagrams of binary titanium alloys, ASM International, Metals Park, Ohio, 1987, 282-284.
[31] L.D. Dudkin, V.I. Vaidanich, The nature of the electrical conductivity of certain compounds of transition metals with $CuAl_2$-type lattices, Sov. Phys.-Sol. State, 2 (1960) 377-378.
[32] S. Bobev, H. Kleinke, Instabilities in the linear Sb atom chain of the new binary antimonide $Ti_{11-x}Sb_{8-y}$, Chem. Mater., 15 (2003) 3523-3529.
[33] H. Kleinke, A three-dimensional extended Sb network in the metallic antimonides (M ',Ti)$_5Sb_8$ (M ' = Zr, Hf, Nb, Mo), Inorg. Chem., 40 (2001) 95-100.
[34] Y. Zhu, H. Kleinke, The new binary antimonide Ti_5Sb_8, Z. Anorg. Allg. Chem., 628 (2002) 2233-2233.
[35] S. Derakhshan, A. Assoud, K.M. Kleinke, E. Dashjav, X. Qiu, S.J.L. Billinge, H. Kleinke, Planar nets of Ti atoms comprising squares and rhombs in the new binary antimonide Ti_2Sb, J. Am. Chem. Soc., 126 (2004) 8295-8302.
[36] A. Tavassoli, A. Grytsiv, F. Failamani, G. Rogl, S. Puchegger, H. Müller, P. Broz, F. Zelenka, D. Maccio, A. Saccone, G. Giester, E. Bauer, M. Zehetbauer, P. Rogl, Constitution of the binary M-Sb systems (M = Ti, Zr, Hf) and physical properties of MSb_2, Intermetallics, 94 (2018) 119-132.
[37] J. Murray, Phase diagrams of binary titanium alloys, ASM International, Metals Park, Ohio, 1987, 294-299.
[38] C. Kuper, W.Q. Peng, A. Pisch, F. Goesmann, R. Schmid-Fetzer, Phase formation and reaction kinetics in the system Ti-Sn, Z. Metallkd., 89 (1998) 855-862.
[39] J.W. O'Brien, R.A. Dunlap, J.R. Dahn, A Mössbauer effect and X-ray diffraction investigation of Ti–Sn intermetallic compounds: I. Equilibrium phases, J. Alloy. Compd., 353 (2003) 60-64.
[40] A.A. Bondar, T.Y. Velikanova, D.B. Borysov, L. Artyukh, O.O. Bilous, M.P. Burka, O.S. Fomichov, N.I. Tsyganenko, S.O. Firstov, Titanium-boride eutectic materials: Phase equilibria and properties of alloys in the Ti-rich portion of the Ti-Sn-B system, J. Alloy. Compd., 400 (2005) 202-208.
[41] F. Hayes, I. Ansara, A. Dinsdale, M. Rands, Thermochemical Database for Light Metal Alloys, COST 507, 2 (1998) 284-287.
[42] C.L. Liu, U.E. Klotz, P.J. Uggowitzer, J.F. Loffler, Thermodynamic assessment of the Sn-Ti system, Monatsh. Chem., 136 (2005) 1921-1930.
[43] F.H. Yin, J.C. Tedenac, F. Gascoin, Thermodynamic modelling of the Ti-Sn system and calculation of the Co-Ti-Sn system, Calphad, 31 (2007) 370-379.
[44] J.A. Wang, C.L. Liu, C. Leinenbach, U.E. Klotz, P.J. Uggowitzer, J.F. Loffler, Experimental investigation and thermodynamic assessment of the Cu-Sn-Ti ternary system, Calphad, 35 (2011) 82-94.
[45] H. Okamoto, Sn-Ti (Tin-Titanium), J. Phase Equilib. Diff., 31 (2010) 202-203.
[46] V.N. Eremenko, T.Y. Velikanova, Study of the tin-titanium system in the high-tin-content region, Russ. J. Inorg. Chem., 7 (1962) 902-904.
[47] Y. Plevachuk, S. Mudry, V. Sklyarchuk, A. Yakymovych, U.E. Klotz, M. Roth, Viscosity and electrical conductivity of liquid Sn-Ti and Sn-Zr alloys, J. Mater. Sci., 42 (2007) 8618-8621.

[48] E. Dashjav, H. Kleinke, Sn/Sb atom ordering in the ternary stannide-antimonide TiSnSb, J. Solid State Chem., 176 (2003) 329-337.
[49] H. Kim, M.M. Olmstead, J.Y. Chan, P.C. Canfield, I.R. Fisher, R.W. Henning, A.J. Schultz, S.M. Kauzlarich, Structure and physical properties of the new pseudo-binary intermetallic compound $Ti_{11}(Sb, Sn)_8$, J. Solid State Chem., 157 (2001) 225-232.
[50] A.J.C. Wilson, International Tables for X-ray Crystallography Kluver, Dordrecht, The Netherlands, 1992.
[51] Z. Otwinowski, W. Minor, Processing of X-ray diffraction data collected in oscillation mode, Methods Enzymol., 276 (1997) 307-326.
[52] B.V. Nonius, Collect, Data collection software, 1999.
[53] G.M. Sheldrick, SHELXS-97, A Program for the Solution of Crystal Structures, University of Göttingen, Germany 1997.
[54] G.M. Sheldrick, SHELXL-97, A Program for Crystal Structure Refinement, University of Göttingen, Germany 1997
[55] G.M. Sheldrick, A short history of SHELX, Acta. Crystallogr. A, 64 (2008) 112-122.
[56] G.M. Sheldrick, SHELXT - Integrated space-group and crystal-structure determination, Acta Crystallogr. A, 71 (2015) 3-8.
[57] E. Dowty, ATOMS, A computer program for displaying atomic structures, 2013.
[58] P. Berger, C. Schmetterer, H.S. Effenberger, H. Flandorfer, The ternary phase $Li_8Sb_xSn_{3-x}$ with $0.3 \leq x \leq 1.0$, Z. Krist.-Cryst. Mater., 235 (2020) 183-192.
[59] P. Berger, H. Flandorfer, Enthalpy of mixing of liquid Li-Sb-Sn alloys, J. Mol. Liq., 298 (2020).
[60] C. Colinet, J.C. Tedenac, Structural stability of ternary $D8_m$-Ti_5Sb_2X (X=Al, Ga, In, Si, Ge, Sn) compounds, Calphad, 49 (2015) 8-18.
[61] J. Lukovic, D. Zagorac, J.C. Schon, J. Zagorac, D. Jordanov, T. Volkov-Husovic, B. Matovic, Tungsten disilicide (WSi_2): synthesis, characterization, and prediction of new crystal structures, Z. Anorg. Allg. Chem., 643 (2017) 2088-2094.
[62] P. Pietrokowsky, P. Duwez, Crystal structure of Ti_5Si_3,Ti_5Ge_3, and Ti_5Sn_3, J. Met., 191 (1951) 772-773.
[63] H. Nowotny, H. Auer-Welsbach, J. Bruss, A. Kohl, Ein Beitrag zur Mn_5Si_3-Struktur ($D8_8$-Typ), Monatsh. Chem., 90 (1959) 15-23.
[64] P. Berger, H. Flandorfer, Sb-Sn alloy anodes for Li-ion batteries: The ternary system Li-Sb-Sn, J. Alloy. Compd., 855 (2021).

Table 1. Single-crystal X-ray data-collection and structure refinements of $Sb_xSn_{19-x}Ti_{15}$ and $(Sb_xSn_{1-x})_{3-y}Ti_{5+y}$. Cell parameter obtained from PXRD are given in brackets.

	T4	T2	$(Sb_xSn_{1-x})_{3+y}Ti_5$	$(Sb_xSn_{1-x})_{3+y}Ti_5$	
	$Sb_xSn_{19-x}Ti_{15}$	$(Sb_xSn_{1-x})_{3-y}Ti_{5+y}$	$(Sb_{0.48}Sn_{0.52})_{3.10}Ti_5$	$(Sb_{0.21}Sn_{0.79})_{3.40}Ti_5$	
a [Å]	8.8502(8), [8.8454(1)]	10.553(15), [10.5347(1)]	8.0643(12), [8.0469(1)]	8.1787(11), [8.1749(1)]	
c [Å]	—	5.3982(8), [5.4025(6)]	5.4718(6), [5.4646(1)]	5.5913(6), [5.5935(1)]	
Space group	$Pm\bar{3}$ (no. 200)	*I*4/*mcm* (no. 140)	$P6_3/mcm$ (no. 193)	$P6_3/mcm$ (no. 193)	
V [Å³]	693.2	601.2	308.2	323.9	
Z	1 $\{Sb_6Sn_{13}Ti_{15}\}$	4 $\{(Sb,Sn)_3Ti_5\}$	2 $\{(Sb,Sn)_4Ti_5\}$	2 $\{(Sb,Sn)_4Ti_5\}$	
Pearson symbol	*cP*34	*tI*32	*hP*18	*hP*18	
Crystal dimensions [µm³]	30×35×50	25×30×40	30×35×45	40×50×55	
Range of data collection ($\pm h$ $\pm k$ $\pm l$) [°]	$3 < 2\vartheta < 70$	$3 < 2\vartheta < 80$	$3 < 2\vartheta < 80$	$3 < 2\vartheta < 80$	
Number of images / rotation angle per image [°]	473 / 2	503 / 2	610 / 2	549 / 2	
Scan time [s/°] / frame size (binned mode) [pixels]	160 / 621×576	200/ 621×576	230 / 621×576	200 / 621×576	
Detector-to-sample distance [mm]	32	32	32	32	
Measured reflections (scan mode φ-scans at 10 distinct ω-angles)	7,303	5,986	2,563	6,975	
Unique reflections (n) / reflections with $F_o > 4\sigma(F_o)$	594 / 573	536 / 475	379 / 368	399 / 376	
$R_{int} = \Sigma \lvert F_o^2 - F_o^2(\text{mean}) \rvert / \Sigma F_o^2$	0.035	0.0223	0.017	0.042	
Extinction parameter k: $F_c^* = F_c \cdot k[1+0.001 \cdot F_c^2 \lambda^3/\sin(2\vartheta)]^{-1/4}$	0.00336(16)	0.00050(12)	0.0057(9)	0.0020(5)	

$R1 = \Sigma(\lvert\lvert F_o\rvert - \lvert F_c\rvert\rvert) / \Sigma F_o$ (all / observed reflections)	0.0167 / 0.0155	0.023 / 0.018	0.020 / 0.019	0.0020(5)	
$wR2 = [\Sigma w(F_o^2-F_c^2)^2 / \Sigma \lvert wF_o^4]^{1/2}$	0.035	0.038	0.049	0.056	
GooF = $\{\Sigma[w(F_o^2-F_c^2)^2] / (n-p)\}^{0.5}$	1.29	1.10	1.13	1.15	
Max Δ/σ; number of variable parameters (p)	< 0.001; 21	< 0.001; 18	< 0.001; 17	< 0.001; 17	
Weighting parameter a / b	0.01 / 0.167	0.015 / 2.28	0.033 / 0.28	0.021 / 2.89	
Final difference Fourier map [eÅ^{-3}]	-1.02 to +0.88	-1.37 to +1.88	-1.33 to +1.26	-1.63 to +2.47	

$w = 1 / \{ \sigma^2(F_o^2) + [a \times P]^2 + b \times P\}$; $P = ([\max(0,F_o^2)] + 2 \times F_c^2) / 3]$

Table 2. Fractional atomic coordinates and displacement parameters of $Sb_xSn_{19-x}Ti_{15}$, $(Sb_xSn_{1-x})_{3-y}Ti_{5+y}$, $(Sb_{0.48}Sn_{0.52})_{3.10}Ti_5$, and $(Sb_{0.21}Sn_{0.79})_{3.40}Ti_5$. The anisotropic displacement parameters are defined as: $\exp[-2\pi^2 \Sigma^3_{i=1} \Sigma^3_{j=1} U_{ij}\ a^*_i\ a^*_j\ h_i\ h_j]$.

atom	site occupation	Wyckoff letter	site symmetry	*x*	*y*	*z*	U_{equiv} / U_{iso}	U_{11}	U_{22}	U_{33}	U_{23}	U_{13}	U_{12}
$Sb_xSn_{19-x}Ti_{15}$													
*M*1	$Sn_{1.0}$	1(*a*)	$m\bar{3}.$	0	0	0	0.01224(13)	0.01224(13)	= U_{11}	= U_{11}	0	0	0
*M*2	$Sb_{1.0}$	6(*h*)	*mm*2 ..	0.17323(3)	0.5	0.5	0.00746(7)	0.00736(11)	0.00757(11)	0.00744(11)	0	0	0
*M*3	$Sn_{1.0}$	12(*j*)	*m*..	0	0.32317(2)	0.18401(2)	0.01060(7)	0.00722(9)	0.01507(10)	0.00950(9)	0.00325(6)	0	0
Ti1	$Ti_{1.0}$	1(*b*)	$m\bar{3}.$	0.5	0.5	0.5	0.0057(3)	0.0057(3)	0.0057(3)	0.0057(3)	0	0	0
Ti2	$Ti_{1.0}$	6(*g*)	*mm*2 ..	0.21368(8)	0.5	0	0.00803(12)	0.00793(3)	= U_{11}	= U_{11}	0	0	0
Ti3	$Ti_{1.0}$	8(*i*)	.3.	0.29773(4)	= *x*	= *x*	0.00753(11)	0.00753(11)	= U_{11}	= U_{11}	-0.00038(11)	= U_{23}	= U_{23}
$(Sb_xSn_{1-x})_{3-y}Ti_{5+y}$													
*M*1	$Sn_{0.861(3)}Ti_{0.139}$	4(*a*)	422	0	0	0.25	0.00940(9)	0.00888(11)	= U_{11}	0.01045(17)	0	0	0.00940(9)
*M*2	$Sb_{0.988(3)}Ti_{0.012}$	8(*h*)	*m*.2*m*	0.16373(9)	= *x* + 0.5	0	0.00862(7)	0.00697(8)	= U_{11}	0.01194(12)	0	0	-0.00036(6)
Ti1	$Ti_{1.0}$	4(*b*)	$\bar{4}2m$	0	0.5	0.25	0.00853(16)	0.00922(2)	= U_{11}	0.00723(3)	0	0	0
Ti2	$Ti_{1.0}$	16(*k*)	*m*..	0.07735(4)	0.22712(4)	0	0.01029(12)	0.00714(18)	0.00925(19)	0.01452(2)	0	0	-0.00006(12)
$(Sb_{0.48}Sn_{0.52})_{3.10}Ti_5 = M_{3.10}Ti_5$													
M1	$Sb_{1.0}$	*m*2	6(*g*)	0.60959(3)	0	1/4	0.01141(9)	0.01230(10)	0.00863(11)	0.01208(12)	0	0	= 1/2 U_{11}

		m											
Ti1	$Ti_{0.995(5)}$	*mm2*	6(*g*)	0.24647(12)	0	1/4	0.0215(2)	0.0261(3)	0.0114(3)	0.0220(3)	0	0	= 1/2 U_{11}
Ti2	$Ti_{0.995(5)}$	3.2	4(*d*)	1/3	2/3	0	0.00911(17)	0.0096(2)	= U_{11}	0.0081(2)	0	0	= 1/2 U_{11}
*M*2	$Sb_{0.107(2)}$	$\bar{3}$	2(*b*)	0	0	0	0.0091(8)	0.0082(9)	= U_{11}	0.0109(12)	0	0	= 1/2 U_{11}
$(Sb_{0.21}Sn_{0.79})_{3.40}Ti_5 = M_{3.40}Ti_5$													
M1	$Sb_{1.0}$	*m2m*	6(*g*)	0.61059(4)	0	1/4	0.01010(10)	0.00958(12)	0.00771(14)	0.01237(15)	0	0	= 1/2 U_{11}
Ti1	$Ti_{1.022(8)}$	*mm2*	6(*g*)	0.26473(16)	0	1/4	0.0221(3)	0.0146(4)	0.0100(4)	0.0403(8)	0	0	= 1/2 U_{11}
Ti2	$Ti_{1.030(7)}$	3.2	4(*d*)	1/3	2/3	0	0.0088(3)	0.0093(3)	= U_{11}	0.0078(4)	0	0	= 1/2 U_{11}
*M*2	$Sb_{0.443(4)}$	$\bar{3}$	2(*b*)	0	0	0	0.0076(3)	0.0071(3)	= U_{11}	0.0088(5)	0	0	= 1/2 U_{11}

Table 3. Interatomic bond distances (in Å) for $Sn_{19-x}Sb_xTi_{15}$ and $(Sb_xSn_{1-x})_{3-y}Ti_{5+y}$.

$Sb_xSn_{19-x}Ti_{15}$				$(Sb_xSn_{1-x})_{3-y}Ti_{5+y}$	
*M*1—*M*3	3.2913(4), 12x	Ti1—*M*2	2.8920(4), 6x	*M*1—*M*1	2.6991(4), 2x
		Ti1—Ti3	3.1006(7), 8x	*M*1—Ti2	2.8692(5), 8x
*M*2—Ti3	2.761(4), 4x				
*M*2—Ti1	2.8920(4)	Ti2—*M*3	2.9458(6), 4x	*M*2—Ti1	2.7912(4), 2x
*M*2—Ti2	2.9617(7), 2x	Ti2—*M*3	2.9597(4), 2x	*M*2—Ti2	2.7925(6), 2x
*M*2—*M*2	3.0663(6)	Ti2—*M*2	2.9617(7), 2x	*M*2—Ti2	2.8133(6), 2x
*M*2—*M*3	3.5525(4), 4x	Ti2—Ti3	3.2712(4), 4x	*M*2—Ti2	3.0729(4), 4x
		Ti2—Ti2	3.7822(15)	*M*2—*M*2	3.7308(5), 2x
*M*3—Ti3	2.8296(5), 2x				
*M*3—Ti2	2.9458(6), 2x	Ti3—*M*2	2.7610(4), 3x	Ti1—Ti1	2.6991(4), 2x
*M*3—Ti2	2.9597(4)	Ti3—*M*3	2.8296(5), 3x	Ti1—*M*2	2.7912(4), 4x
*M*3—*M*3	3.1299(5)	Ti3—Ti1	3.1006(7)	Ti1—Ti2	3.2833(6), 8x
*M*3—*M*3	3.2571(5)	Ti3—Ti2	3.2712(4), 3x		
*M*3—*M*1	3.2913(4)	Ti3—Ti3	3.5803(8), 3x	Ti2—*M*2	2.7926(6)
*M*3—*M*3	3.5142(4), 4x			Ti2—*M*2	2.8133(6)
				Ti2—*M*1	2.8692(5), 2x
				Ti2—Ti2	2.9181(10)
				Ti2—*M*2	3.0729(4), 2x
				Ti2—Ti2	3.1544(6), 2x
				Ti2—Ti1	3.2833(6), 2x

Table 4. Interatomic bond distance up to 4.2 Å (in Å) for $(Sb_{0.21}Sn_{0.79})_{3.40}Ti_5$ and $(Sb_{0.48}Sn_{0.52})_{3.10}Ti_5$.

$(Sb_{0.48}Sn_{0.52})_{3.10}Ti_5$		$(Sb_{0.21}Sn_{0.79})_{3.40}Ti_5$
M1—Ti1	2.7577(5) 2x	2.8170(6) 2x
M1—Ti2	2.8411(3) 4x	2.8890(4) 4x
M1—Ti1	2.9283(10)	2.8287(14)
M1—Ti1	2.9719(5) 2x	2.9758(5) 2x
M1—*M1*	3.2572(4) 2x	3.3299(5) 2x
M1—*M*2	3.4327(5) 2x	3.4781(5) 2x
Ti1—*M*2	2.4129(8) 2x	2.5772(11) 2x
Ti1—*M1*	2.7577(5) 2x	2.8170(6) 2x
Ti1—*M1*	2.9283(10)	2.8287(14)
Ti1—*M1*	2.9719(5) 2x	2.9758(5) 2x
Ti1—Ti1	3.3817(6) 4x	3.5360(8) 4x
Ti1—Ti2	3.3869(7) 4x	3.3512(8) 4x
Ti1—Ti1	3.4427(17) 2x	3.750(2) 2x
Ti2—Ti2	2.7359(3) 2x	2.7956(3) 2x
Ti2—*M1*	2.8411(3) 6x	2.8890(4) 6x
Ti2—Ti1	3.3869(7) 6x	3.3512(8) 6x
*M*2—Ti1	2.4129(8) 6x	2.5772(11) 6x
*M*2—*M*2	2.7359(3) 2x	2.7956(3) 2x
*M*2—*M1*	3.4327(5) 6x	3.4781(5) 6x

Table 5: Composition and temperature ranges of the four ternary compounds T1, T2, T3 and T4 found in this work.

Phase designation	**T1**	**T2**	**T3**	**T4**
Structured formula	SbSnTi	$(Sb_xSn_{1-x})_{3-y}Ti_{5+y}$	Sb_4SnTi_5	$Sb_xSb_{19-x}Ti_{15}$
max. homogeneity range concerning the Sb amount [at.%]	18.8-49.4*	16.1-21.4***	39.4-40.6**	12.7-18.1*
max. homogeneity range concerning the Ti amount [at.%]	33.5-34.0*	64.1-65.0***	50.4-50.8**	44.1-44.6*
Observed at	600°C, 800°C	600°C, 800°C, 1000°C	800°C, 1000°C	600°C

* at 600°C ** at 800°C *** at 1000°C

Credit author statement

P. Berger: Investigation, Validation, Visualization, Writing – Original draft

C. Schmetterer: Investigation, Validation, Writing – Review and Editing

H. S. Effenberger: Investigation, Validation, Visualization, Writing – Original draft

H. Flandorfer: Conceptualization, Validation, Writing – Review and Editing, Supervision, Project administration, Funding acquisition

Declaration of interests

☒ The authors declare that they have no known competing financial interests or personal relationships that could have appeared to influence the work reported in this paper.

☐The authors declare the following financial interests/personal relationships which may be considered as potential competing interests:

Highlights:

- First description of isothermal sections of the ternary intermetallic system Sb-Sn-Ti at 600°C, 800°C and 1000°C
- Critical assessment of a high number of Sb-Sn-Ti alloys investigated by PXRD, SCXRD and SEM/EDX
- Two ternary phases were confirmed and two new ternary phases were discovered
- $Sb_xSn_{19-x}Ti_{15}$ and $(Sb_xSn_{1-x})_{3-y}Ti_{5+y}$ were characterized by SCXRD the first time